Screening of biopolymeric materials for cardiovascular surgery toxicity—Evaluation of their surface relief with assessment of morphological aspects of monocyte/macrophage polarization in atherosclerosis patients

Natalia G. Menzyanova[a], Svetlana A. Pyatina[a], Elena D. Nikolaeva[b], Alexander V. Shabanov[c], Ivan V. Nemtsev[d], Dmitry P. Stolyarov[e], Dmitry B. Dryganov[e], Eugene V. Sakhnov[e], Ekaterina I. Shishatskaya[a,b,]*

[a] Siberian Federal University, 79, Svobodny av., Krasnoyarsk, 660041, Russia
[b] Institute of Biophysics, Siberian Branch of the Russian Academy of Sciences, 50/50 Akademgorodok, Krasnoyarsk, 660036, Russia
[c] L.V. Kirensky Institute of Physics, Siberian Branch of the Russian Academy of Sciences, 50/38 Akademgorodok, Krasnoyarsk, 660036, Russia
[d] Federal Research Center Krasnoyarsk Scientific Center of the Siberian Branch of the Russian Academy of Sciences, 50 Akademgorodok, Krasnoyarsk, 660036, Russia
[e] Federal Center for Cardiovascular Surgery, 45 Karaulnaya, Krasnoyarsk, 660020, Russia

ARTICLE INFO

ABSTRACT

The morphotypes of human macrophages (MPh) were studied in the culture on nano-structured biopolymer substrates, made from polyhydroxyalcanoates (PHAs) of five various monomer compositions, followed by the solvent evaporation. Its surface relief, which was further in direct contact with human cells *in vitro,* was analyzed by atomic force microscopy (AFM) and scanning electron microscopy (SEM). It was shown, that the features of the micro/nano relief depend on the monomeric composition of the polymer substrates. Monocytes (MN) of patients with atherosclerosis and cardiac ischemia, undergoing stenting and conventional anti-atherosclerotic therapy, were harvested prior and after stenting. MN were isolated and cultured, with the transformation into MPh in direct contact with biopolymer culture substrates with different monomer composition and nano-reliefs, and transformed into MPh, in comparison with the same process on standard culture plastic. Sub-populations of cells with characteristic morphology in each phenotypic class were described, and their quantitative ratios for each sample of polymers were counted as an intermediate result in the development of "smart" material for cardiovascular devices.

The results obtained allow us to assume, that the processes of MPh differentiation and polarization *in vitro* depend not only on the features of the micro/nano relief of biopolymer substrates, but also on the initial state of MN *in vivo* and general response of patients.

1. Introduction

The successful development of technologies in regenerative medicine is largely associated with the development of biocompatible, biodegradable and non-toxic materials that are used to make implants [1–3]. *In vitro* screening revealed the positive effect of such materials on the proliferation and differentiation processes of various types of stem and progenitor cells [4–14]. But in the *in vivo* conditions there is one important cell class – macrophages (MPh), which necessarily interact with the implant. As a result of contact interaction with the material, polarization of MPh forms a new microenvironment for progenitor cells and realizes the processes of target histogenesis, which are good observed in model systems *in vitro,* are not always adequately implemented *in vivo*. This is situated due to the fact, that the polarization of MPh and the formation of their functional phenotypes – M1/M2 – are associated with the local production of many molecules that affect the processes of differentiation, proliferation and apoptosis of various cell types [15–17].

In vitro studies indicate that polarization of MPh in the absence of specific inductors in the medium depends on the characteristics of the surface relief profile of the substrate material – implantate [18–23]. Thus, the absence of the "chemical" cytotoxicity of tested materials is not enough to complete prediction of the molecular-cellular processes of histogenesis *in vivo*. An assessment of the "toxicity" of the surface relief is necessary: its influence on the processes of polarization of the MPh and the production of cytokines, which can regulate the processes of proliferation, differentiation and apoptosis of various cell types involved in the regeneration processes.

The evaluation of the "toxicity" of the surface relief acquires particular significance for materials for cardiovascular applications, specifically, which are planned to be used as coatings for vascular stents, in patients with ichemic heart desease thanks to their tighter contact with blood and vessel wall and mass of their use.

The development of atherosclerosis is associated with impaired lipid metabolism. In blood vessels these disorders involve increasing level of lipids, associated with the certain classes of serum lipoproteins. Activation of free radical oxidative modifications of lipids in low-density lipoproteins and induction of the synthesis of specific antibodies to modified low-density lipoproteins lead to the appearance of circulating immune complexes. These disorders are the result of long-term epigenetic rearrangements, leading to changes in the methylation level of the genes, involved in the regulatory signaling of lipid metabolism and genes encoding key enzymes of lipid metabolism [27–29].

Increased lipid level in plasma is considered to be an epigenetic factor, triggering the epigenetic rearrangements of circulating blood cells and endothelial cells of blood vessels. These epigenetic changes lead to formation of atherosclerotic plaques, local formations in the wall of the vessel [30–33].

At the histological level an atherosclerotic plaque consists of a) MN-MPh and lipid-loaded foam cells, originating from the MN-MPh; b) actively proliferating smooth muscle cells; c) lymphocytes; d) developed extracellular matrix with lipid inclusions, and e) a vascular network, developed to a different degree [34–36].

Atherosclerotic plaque is a labile system, whose dynamics determines the individual clinical prognosis. Modeling molecular and cellular events in atherosclerotic plaque using *in vitro* and *in vivo* systems has made a significant contribution to our understanding of principles of atherosclerotic plaque biogenesis and the possibilities of its pharmacological regulation. However, the effectiveness of pharmacological control over the dynamics of atherosclerotic plaques in patients remains relatively low [37]. This is due to the fact, that the therapy is aimed at correcting remote of metabolic consequences of epigenetic rearrangements, which determines the pathogenesis of atherosclerosis.

An elegant engineering solution, bypassing the problem of the epigenetic nature of the disease, was found: a stent, as a rigid framework, is installed in the zone of an atherosclerotic plaque and mechanically widens the lumen of the narrowed vessel. Stent materials can include drugs, inhibiting proliferative activity, thrombus formation, and inflammation. Unfortunately, the mechanical solution of the biological problem did not justify the hopes of clinical medicine, because implants often led to restenosis – the accelerated re-development of an unstable atherosclerotic plaque in the implantation zone. The frequency of restenosis when using drug-eluting stents is from 5 to 10% [38–40].

The inconsistency of the engineering approach confirmed the epigenetic nature of atherosclerosis and stimulated the development of materials, whose biological activity is determined not only by chemical groups, exposed on the surface, but also by the micro- and nano-relief features of the stent material. These materials should regulate the functional activity of MN-MPh with the "atherosclerotic" epigenome and prevent the re-development of molecular and cellular events, leading to restenosis.

Screening the biological activity of such materials in development requires adequate *in vitro* models. We argue that mandatory conditions

for the adequacy of such models are:

- the use of MN-MPh cultures as main cell components in the biogenesis of atherosclerotic plaque;
- the isolation of MN from the blood of patients with clinically diagnosed arteriosclerosis of blood vessels, not from healthy donors' blood.

Epigenomic studies call into question the legitimacy of extrapolating the interpretation of cellular responses in health to pathological conditions. Furthermore, contact cultivation of MN-MPh with the material of implants *in vitro* will allow to evaluate individual features of cell interaction and to predict intravascular reactions to implants [41,42].

At the first stage of screening the choice of integral parameters for the assessment of cell-material interaction is crucial. For MN-MPh their morpho-functional polarization can be used as such an integral parameter. M1-polarization leads to the formation of a pro-inflammatory MPh phenotype, when cells are characterized by an elongated form and increased expression of CD40 and CD64. M2-polarization is associated with the formation of an anti-inflammatory MPh phenotype, where round-shaped cells express an elevated level of the mannose receptor and CD163. The dynamics of the ratio of M1/M2 was shown to play a key role in the pathogenesis of various diseases, in particular, of atherosclerosis [43–45].

In vitro and *in vivo* models allow to control MN-MPh polarization by various growth factors (M-CSF, macrophage colony-stimulating factor or GM-CSF, granulocyte-macrophage colony-stimulating factor), cytokines (interleukins IL-4, IL-10), interferon-γ/lipopolysaccharides, dexamethasone [46–48]. Another prospective approach is polarization control using biopolymer materials with various micro- and nano-relief through the mechanochemical signaling [49]. This type of signaling is associated with local changes in the curvature of the cell membrane in contact with the relief of the extracellular matrix or with the culture substrates or scaffolds. Membrane deformations alter the activity of membrane-bound proteins and trigger signaling process. Mechanochemical signaling triggers reorganization of the cytoskeleton and associated changes in cellular morphology. Furthermore, it is involved in the regulation of proliferation, differentiation, and apoptosis of cells [50–54].

This determines the important role of mechanochemical signaling in the regulation of epigenetic rearrangements. Targeting regulatory signalling by features of micro- and nano-relief and transmission of topographic information into epigenome rearrangements is one of the most promising approaches in the development of polymeric materials for regenerative medicine, in particular, in the technologies of development of bio-active vascular grafts, including vascular stents [55,56].

Therefore, our study focused on morphological aspects of the polarization of MN-MPh, isolated from patients with atherosclerosis and on biodegradable polymeric materials of various compositions, promising for the production of vascular implants. We used the class of natural materials, polyhydroxyalkanoates (PHAs), with various monomeric compositions and different topography to assess the prospects of their application in intravascular stenting in patients with atherosclerosis.

2. Materials and methods

2.1. PHAs polymers

Samples of PHAs were obtained in the process of microbiological synthesis with the cultivation of *Cupriavidus eutrophus B-10646* in specific growth conditions in the Laboratory of Biotechnology of New Materials, Siberian Federal University, as described previously [57]. Samples contained the following monomers: 3-hydroxybutirate, 3-hydroxyvalerate, 4-hydroxybutyrate, 3-hydroxyhexanoate.

Biopolymer samples with the following composition were used in the study:

Sample 1: poly-3-hydroxybutyrate, **P(3HB)**, scaffold 1.

Sample 2: copolymers of 3-hydroxybutyrate and 3-hydroxyvalerate, **P(3HB/3HV)**, scaffold 2.

Sample 3: copolymers of 3-hydroxybutyrate and 4-hydroxybutyrate, **P(3HB/4HB)**, scaffold 3.

Sample 4: copolymers of 3-hydroxybutyrate, 3-hydroxyvalerate and 3-hydroxyhexanoate, **P(3HB/3HV/3HHx)**, scaffold 4.

Sample 5: copolymers of 3-hydroxybutyrate, 3-hydroxyvalerate, 4-hydroxybutyrate and 3-hydroxyhexanoate, **P(3HB/3HV/4HB/3HHx)**; scaffold 5.

Molecular weight and molecular-weight distribution of PHAs were examined using a gel permeation chromatograph ("Agilent Technologies" 1260 Infinity, U.S.) with a refractive index detector, using an Agilent PLgel Mixed-C column. Chloroform was the eluent, at a flow rate of 1.0 ml/min at 40 °C. Typical sample volumes were 50 μl at a polymer concentration of 2 mg/ml. Narrow polydispersity polystyrene standards (Agilent, U.S.) were used to generate a universal calibration curve, from which molecular weights (weight average, Mw, and number average, Mn) and polydispersity (PD) were determined.

Thermal analysis of PHA specimens was performed using a DSC-1 differential scanning calorimeter (METTLER TOLEDO, Switzerland). Powdered polymeric samples (4.0 ± 0.2 mg each) were placed into the aluminum crucible and compressed prior to measurement. Every sample was measured at least 3 times. Samples were preheated to 60 °C and cooled to 25 °C. The specimens were heated to temperatures from 25 °C to 300 °C at 5 °C × min-1 (measurement precision 1.5 °C); melting point (T_{melt}) and thermal decomposition temperature (T_{degr}) were determined from exothermal peaks in thermograms. The thermograms were analyzed using the STARe v11.0 software.

Crystallinity (C_x) was determined using diffractometer D8 ADVANCE (Bruker AXS, Germany) with a linear detector VANTEC, film samples 2 cm in diameter and 0.15 mm thick were prepared from a 2% polymer solution in chloroform. The samples had a circular shape because during measurement the sample spins in a direction perpendicular to the surface. X-Ray structure analysis and determination of crystallinity of PHAs were performed employing a D8ADVANCE X-Ray powder diffractometer equipped with a VANTEC fast linear detector, using CuKa radiation ("Bruker, AXS", Germany). The scan step was 0.016°, measurement time in each step 114 s, and scanning range from 5° to 60° (from 48° to 60° there only was a uniformly decreasing background); the registered parameter was intensity of X-rays scattered by the sample; 55°/0.016° = 3438 times. The degree of crystallinity was calculated as a ratio of the total area of crystalline peaks to the total area of the radiograph (the crystalline + amorphous components). Measurement accuracy: point measurement accuracy ± 0.4 PPS, with the lowest intensity 1.5 PPS and the highest intensity 32 PPS; the error in determination of the degree of crystallinity, which was calculated based on multiple measurements, was 2% or less.

Films were obtained by pouring polymer solutions in chloroform, followed by the solvent evaporation. Homogeneous solutions containing 10–20 g/l polymers were heated to 35 °C and poured into defatted surface of Petri dishes and dried for 2–3 days at room temperature in the laminar box; finally films were dried to constant weight in a vacuum cabinet (Labconco, USA).

The surface characteristics of the films were evaluated using a contact angle measuring device DSA-25E (Krüss, Germany) using DSA-4 Windows software; the water contact angles were measured in the automatic mode; the video frame of the drop was processed in a semi-automatic mode after its stabilization by the "Circle" method built into the software package. The free surface energy, the polar component (mN/m) were calculated by Owens–Wendt–Rabel–Kaelble method using the obtained values of water contact angles. The scaffold surface microstructure was investigated by a scanning electron microscope. Samples with the size of 5 × 5 mm were preliminarily placed on a stage

Table 1

Physicochemical properties of samples PHAs used for the film production.

PHAs composition, mol.%	Polymer characteristics				
	M_n, kDa	M_w, kDa	$C_{x,}$ %	$T_{melt.}$ °C	$T_{degr.}$ °C
P3HB, 100.0	657	1 200	74	167.6	273.8
P(3HB/3 HV) 89.5/10.5	220	695	59	173.2	283.5
P(3HB/4HB) 92/8	580	1 100	42	162.2	268.4
P(3HB/3 HV/3HHx) 66.4/23.4/10.2	589	540	60	176	271
P(3HB/3 HV/4HB/3HHx) 63.5/ 19.4/ 12.3 /4.8	72	437	30	168	286

and sputtered with platinum using an Emitech K575X (Quorum Technologies Limited, UK); SEM images were obtained using TM (Hitachi, Japan). Surface roughness was determined using AFM in a semi-contact mode (Russia). The average (R_a) and root-mean-square roughness (R_q) were calculated at 10 points as the arithmetic average of the absolute values of the height deviations of the 5 highest and 5 deepest points from the midline of the profile using standard equations (Roughness parameters of the same name, ISO 4287/1). The sections with a size of 20 × 20 μm were examined, then sections of 2 × 2 μm of local maxima and minima were selected and analyzed repeatedly with higher resolution, roughness for each sample was calculated for the three sections.

2.2. Patients

Patients of the Cardiology Center in Krasnoyarsk, aged 60–70 and diagnosed coronary heart disease participated in the study. Studies were carried out with the permission of the Ethics Committee of the Cardiology Center with the agreement, signed by those who participated in the studies. Prior to hospitalization, patients were prescribed traditional therapy for cardiac ischemia: acetylsalicylic acid, statins (atorvastatinum or simvastatinum), beta-blockers, calcium antagonists. Patients were prescribed clopidogrel 5 days prior to hospitalization.

One day after the hospitalization, transluminal balloon angioplasty was performed with 2nd-generation stents with everolimusum (Promus Element plus, Boston Scientific Corporation, USA, or Xience Xpedition, ABBOT VASCULAR, USA). After the operation, patients were prescribed disaggregant therapy, statins and beta-blockers.

Venous blood was collected from each patient (20 ml, anticoagulant – EDTA twice: the day before stenting and the day after stenting.

2.3. MN isolation

MN were isolated in the hypertonic density gradient of ficoll-verografin by the method of Recalde H. [58]. The pre-prepared leukomass was layered on a hypertonic gradient (specific density $1.080 \, g/cm^3$) and centrifuged at 400 g for 15 min. The MN fraction from the interphase was washed twice with phosphate buffer (pH = 7.0) (Amresco, USA) and centrifuged at 400 g for 10 min.

The cell concentration was determined in the Goryaev chamber. Cells were suspended in DMEM (Gibco, ThermoFisher Scientific, USA) with 10% fetal bovine serum (FBS) (HyClone, USA) and adjusted to 2×10^6 cells/ml (10^5 cells in 50 μl).

Polymeric films of different composition were placed in culture wells 96-well plates (TPP, Switzerland), then 100 μl of DMEM medium with 10% FBS and 50 μl of cell suspension (in each well 10^5 cells) was added. Polystyrene culture plates served as control. The cells were cultured in a CO_2 incubator (New Brunswick Scientific Eppendorf, USA) for 6 days. Every 3 days the medium was changed. After finishing incubation MTT assay was performed and samples were prepared for morphological analysis using SEM.
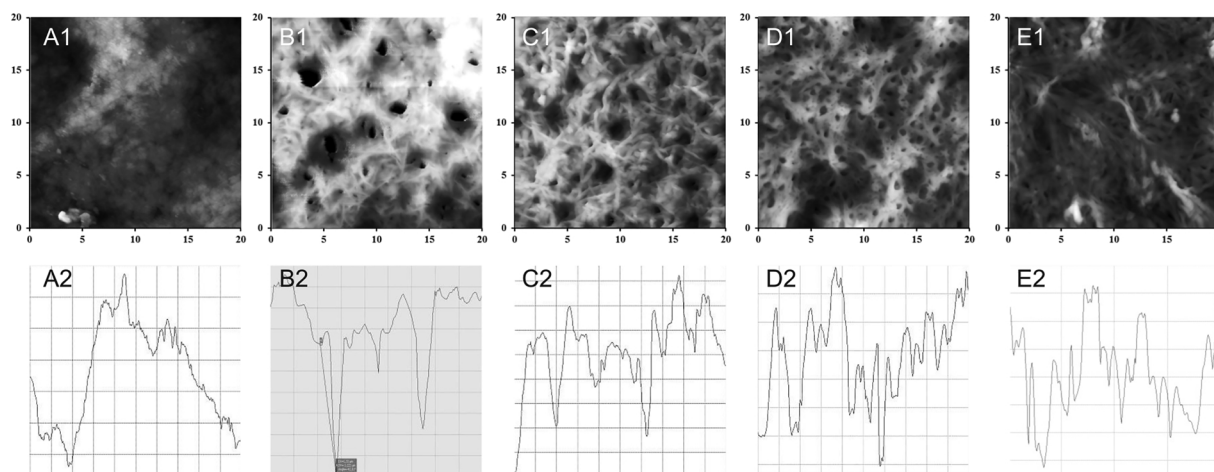
Fig. 1. 3-D Surface topography of biopolymer scaffolds. A – P(3HB) (scaffold 1); B – P(3HB/4HB) (scaffold 2); C – P(3HB/3 HV) (scaffold 3); D – P(3HB/3 HV/3HHx) 66.4/23.4/10.2 (scaffold 4); E – P(3HB/3 HV/4HB/3HHx) 63.5/19.4/12.3/4.8 (scaffold 5). A1-E1 – 3-D reconstructions of surface topography of scaffolds (surface areas 20 μm × 20 μm). A2-E2 – cross-sectional profiles of permanent topography of scaffolds. Abscissae axis is plane, 20 μm for all variants A2-E2. Ordinates axis is the relief depth for A2 – [50–350 nm]; B2 – [400–2400 nm]; C2 – [100–900 nm]; D2 – [400–1100 nm]; E2 – [300–1000 nm].

Table 2
Surface properties of the films with different compostion.

PHA composition, mol. %	Water contact angle, θ, °	Surface free energy, erg/cm²	Polar component of surface free energy, erg/cm²	R_a, arithmetic mean surface roughness, nm	R_q, root mean square roughness, nm	R_z, height of the surface irregularities
P3HB 100.0	97.42 ± 2.6	30.43 ± 1.01	1.23 ± 0.18	71.75	80.28	184.03
P(3HB/3 HV) 85.0/15.0	88.00 ± 2.4	36.90 ± 0.24	2.40 ± 0.09	172.37	206.06	516.36
P(3HB/4HB) 92.0/8.0	78.62 ± 1.2	44.52 ± 1.08	4.24 ± 0.14	177.56	248.10	1260.65
P(3HB/3 HV/3HHx) 66.4/23.4/10.2	89.80 ± 1.6	36.76 ± 1.10	1.90 ± 0.12	158.26	198.50	754.05
P(3HB/3 HV/4HB/ 3HHx) 63.5/ 19.4/ 12.3 /4.8	97.98 ± 1.9	25.82 ± 1.25	1.58 ± 0.42	120.91	157.54	728.63

2.4. MTT assay

At the end of the incubation the culture medium was removed from the wells and the cells were washed with fresh DMEM medium with 10% FBS. 200 μl of MTT solution (Sigma-Aldrich, USA) in DMEM medium with 10% FBS (final MTT concentration 0.25 mg/ml) was added to the wells. The cells were incubated for 4 h. After the incubation the medium was replaced by 150 μl of DMSO (Amresco, USA). Aliquots of 100 μl were transferred to clean plates and the optical density was determined at λ = 550 nm on a multichannel reader iMark™ Microplate Absorbance Reader (Bio-Rad, USA).

2.5. SEM

After cell incubation the culture medium was removed from the wells and the cells were fixed with 2.5% glutaraldehyde (Sigma-Aldrich, USA) in phosphate buffer (Amresco, USA) for 2 h. The cells in the wells were additionally fixed with 1% OsO₄ (SPI Supplies, Structure Probe, Inc., USA) for 40 min. After that biopolymer-cell samples were washed and passed through ethanol with increasing concentration (from 10% to 100% ethanol with step 10%). Biopolymer-cell samples were taken out from the wells. In the control variant the bottom of the wells was cut out and fixed on aluminum foil or on metal object tables.

The samples were analyzed using SEM TM 3000 (Hitachi, Japan). Prior to microscopy the samples were sputter coated with platinum (3

cycles at 10 mA for 20 s) with an Emitech K575X sputter coater (Quorum Technologies, England).

2.6. Statistics

Statistical analysis of the results was performed by conventional methods, using the Microsoft Excel software package. Arithmetic means and standard deviations were found. The statistical significance of results was determined using Student's test (significance level: P ≤ 0.05). Statistical analysis of surface properties of the samples was performed by using embedded methods of the DSA-4 software.

3. Results

3.1. The basic physicochemical properties of PHAs

The five types of PHA polymers, used for the films casting had different basic physicochemical properties. Copolymers with the predominance of 3HB monomers, similar to homopolymer of P(3HB), had similar melting points (162–160 °C) and thermal degradation temperatures (268–273 °C), as well as weight average molecular weight (1100000–1200000 Da); the exception was the copolymer P(3HB/3HH) which had M_w values almost half the rest of the samples (Table 1).

One of the important biological characteristics of implants is the wettability of their surface by polar and nonpolar liquids which is

Table 3

Morphological classes and morphotypes of MPh on the 6th day of cultivation on standard culture plastics and biopolymer scaffolds of various composition. MN were isolated from the patient's blood before the stent was installed and after the stent was installed. MN were cultivated on culture plastic and on biopolymers scaffolds of various compositions (scaffolds 1, 2, 3, 4, 5) in 96-well culture plates (10^5 cells/well) in DMEM medium with 10% fetal serum in CO_2-incubator. After 6 days of culture the cells were fixed in the wells of the plate with 2.5% glutaraldehyde and samples were prepared for SEM using a standard protocol.

Experimental condition	Morphological classes, % of total cell number						
	Morphological class 1 Rounded cells		Morphological class 2 Elongated cells				Morphological class 3 Cells with unusual morphology
	Morphotype 1 Multinuclear cells	Morphotype 2 Mononuclear cells	Morphotype 1 Filiform cells	Morphotype 2 Spindle-shaped cells	Morphotype 3 Rod-shaped cells	Morphotype 4 «Triangular» cells	
Culture plastic, before stenting	19.75	28.18	3.50	26.75	5.73	15.13	0.96
Culture plastic, after stenting	19.10	35.76	1.04*	30.90	9.72*	3.13*	0.35*
Scaffold 1, before stenting	15.98	18.14	6.26	43.20	9.94	2.59	3.89
Scaffold 1, after stenting	20.49	22.97	9.19*	33.22	6.01*	1.77*	6.36*
Scaffold 2, before stenting	10.87	54.35	1.09	23.91*	3.26	3.26	3.26
Scaffold 2, after stenting	11.51	9.47*	17.99*	50.00	6.24*	0	2.52
Scaffold 3, before stenting	9.30	46.51	3.10	30.23	5.43	4.65	0.78
Scaffold 3, after stenting	4.17*	37.50	4,.17	41.67	8.33*	4.17	0.00
Scaffold 4, before stenting	14.98	20.70*	8.81	36.56	10.57	6.17	2.20
Scaffold 4, after stenting	5.45*	13.64	3.64*	60.91*	6.36*	7.27	2.73
Scaffold 5, before stenting	10.48	31.43	3.81	37.14	11.43	5.71	10.48
Scaffold 5, after stenting	17.74	40.32	4.84	29.03	3.23*	3.23*	1.61*

An asterisk indicates the cases where the value after the stent installation (before stenting) was significantly different from the value before the stent installation (after stenting) ($p \leq 0.05$).
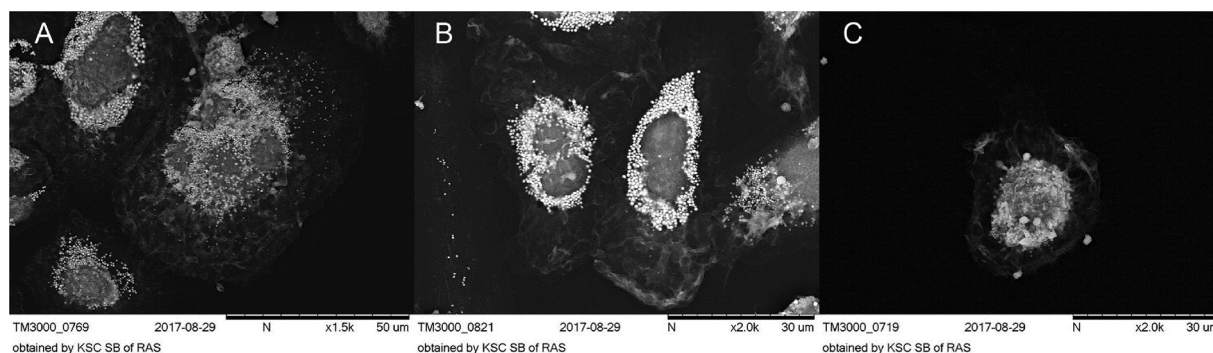
Fig. 2. Morphotypes of the 1st morphological class. 6 days, culture plastic. A, B – morphotype of multinuclear cells. Large cells with numerous lipid droplets in the cytoplasm. Nuclei are seen as gray, rounded structures against the background of high-contrast lipid droplets. C – morphotype of mononuclear cells. Both morphotypes have a complex relief of the plasma membrane.
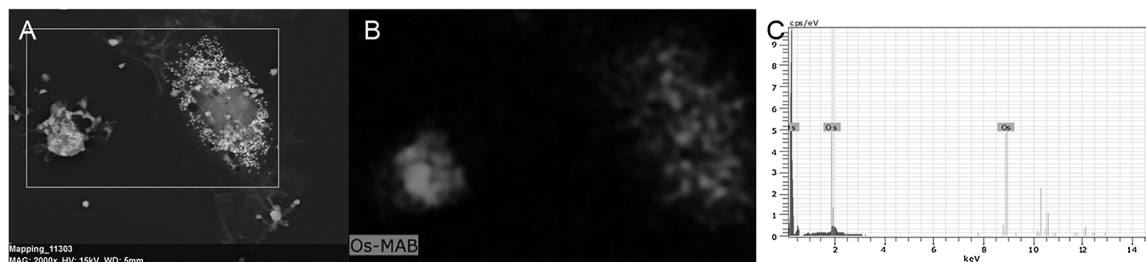
Fig. 3. X-ray spectral analysis of MPh. A – area selected for analysis. B – area of osmium localization (red zones). C – characteristic spectral lines of osmium.
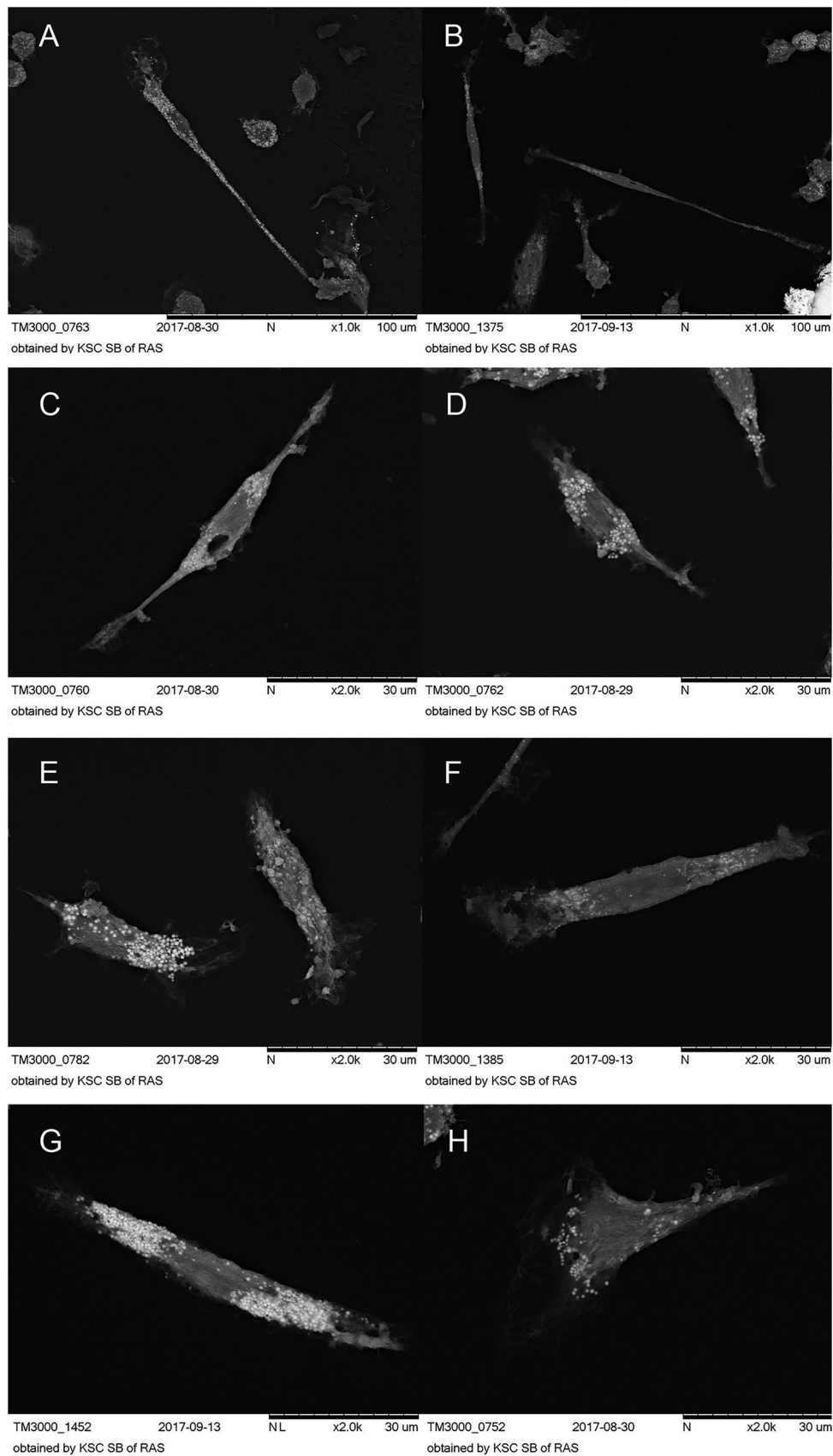
Fig. 4. Morphotypes of the 2nd morphological class. 6 days, culture plastic. A, B – morphotype of filamentous cells; long, "thin" cells, the length varies from 80 μm to 150 μm (indicated by white arrows). C, D – morphotype of spindle-shaped cells; relatively "short" cells with a pronounced central spindle-shaped thickening. E, F, G – morphotype of rod-shaped cells; elongated cells of approximately the same diameter along the entire length. F – morphotype of triangular cells. Lamellopodia with complex surface relief of the plasma membrane, located at the poles were observed for all 4 morphotypes. Magnification: x1000 (A, B), x2000 (C, D, E, F).
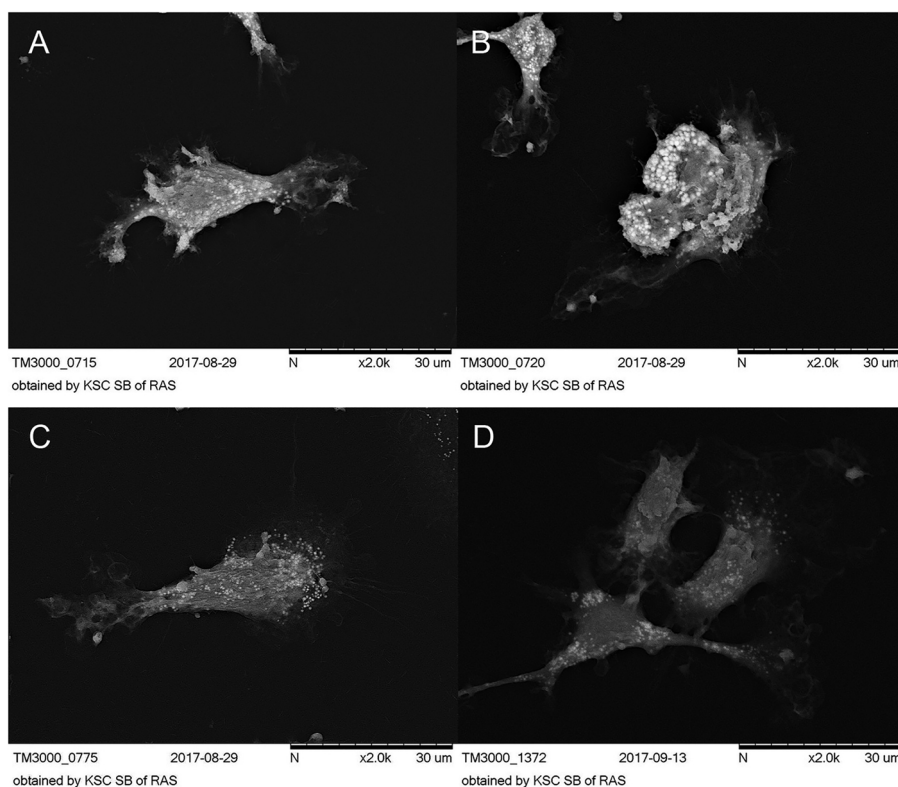
Fig. 5. Morphotypes of the 3rd morphological class (unusual morphology). 6 days, culture plastic. A, B, C, D – variants of the 3rd morphological class morphotypes.

determined by the value of the contact angle. A comprehensive assessment of both helps to predict biocompatibility of material in direct contact with cells. The value of the contact angle of water wetting for the copolymer films was from 78.65 to 97.98 ° with the minimum value for P(3HB/4HB); this is lower than for homopolymer films (97.42) and control (92.46) which indicates a favorable effect of the monomers other than 3HB on the wettability. The P(3HB) homopolymer films and the P(3HB/3 HV/4HB/3HHx) copolymer films had the same wettability.

Surface roughness is the most important parameter for implantable biomaterials, determining the adhesion, spreading and motor activity of cells, the biosynthesis of specific proteins and mechanochemical signaling. The study of the film surface roughness showed significant differences in film samples of different composition: height of the surface irregularities was significantly different from that of P3HB – the deviation of the roughness profile of the copolymers was almost 2.5 times higher than that of the homopolymer. The root-mean-square roughness maximum was 248 nm in P(3HB/4HB); minimal value was 157 for 4-component sample, with respect to 80 nm for P3HB (Fig. 1, Table 2).

3.2. Cell morphology on different culture substrates

Based on microscopic analysis of cells in different experimental conditions two basic morphological classes were identified: 1 – rounded cells; 2 – elongated cells. Cells with unusual morphology (a small percentage of the cell population) were classified as class 3 (Table 3).

In the 1st morphological class two morphotypes were identified:

- rounded, single-nucleated cells
- large rounded cells with several nuclei.
- In the 2nd morphological class four morphotypes were identified:
- filamentous cells: strongly elongated cells, the length is many times greater than the transverse diameter
- spindle-shaped cells: elongated cells with spindle-shaped thickening

in the middle of the cell body
- rod-shaped cells: elongated cells with the same transverse diameter throughout the cell body
- triangular cells: cells of triangular shape with one highly elongated apex.

Rounded form (the 1st morphological class) was referred to as stationary cells, elongated form (the 2nd morphological class) was referred to as mobile cells.

This classification was used to assess the morphological diversity of macrophages in control (culture plastic) and on PHAs-biopolymer substrates of different monomer composition.

3.2.1. MN-MPh culture on culture plastic

3.2.1.1. MPh obtained from MN, isolated before stent placement. On the 6th day of cultivation the number of two main morphological classes of MPh (rounded cells and elongated cells) was the same: 47.9% and 51.1% respectively (Table 1). Among the rounded cells, relatively small single-nucleated cells predominated (Fig. 2 c). In large rounded cells 2-3 nuclei were observed (Fig. 2a, b). They stood out as dark rounded formations against the backdrop of numerous lipid droplets in the cytoplasm. Lipid drops in the cytoplasm were detected as numerous, very contrasting, nanosized vesicular structures. X-ray spectral analysis of cell samples showed that these vesicular structures colocalized with the sites of local concentration of osmium (Fig. 3 a, b). OsO_4 is known to bind phospholipids in the region of the polar heads and interact with the double bonds of fatty acid residues in the lipids to form osmate esters [59]. This determines the concentration of osmium in the lipid droplets and their high contrast.

In the morphological class of elongated cells two morphotypes dominated: spindle-shaped cells (26.75%) (Fig. 4 c, d) and triangular cells (15.13%) (Fig. 4 g).

3.2.1.2. MPh obtained from MN, isolated after stent placement. In this experimental condition on the 6th day of cultivation the number of
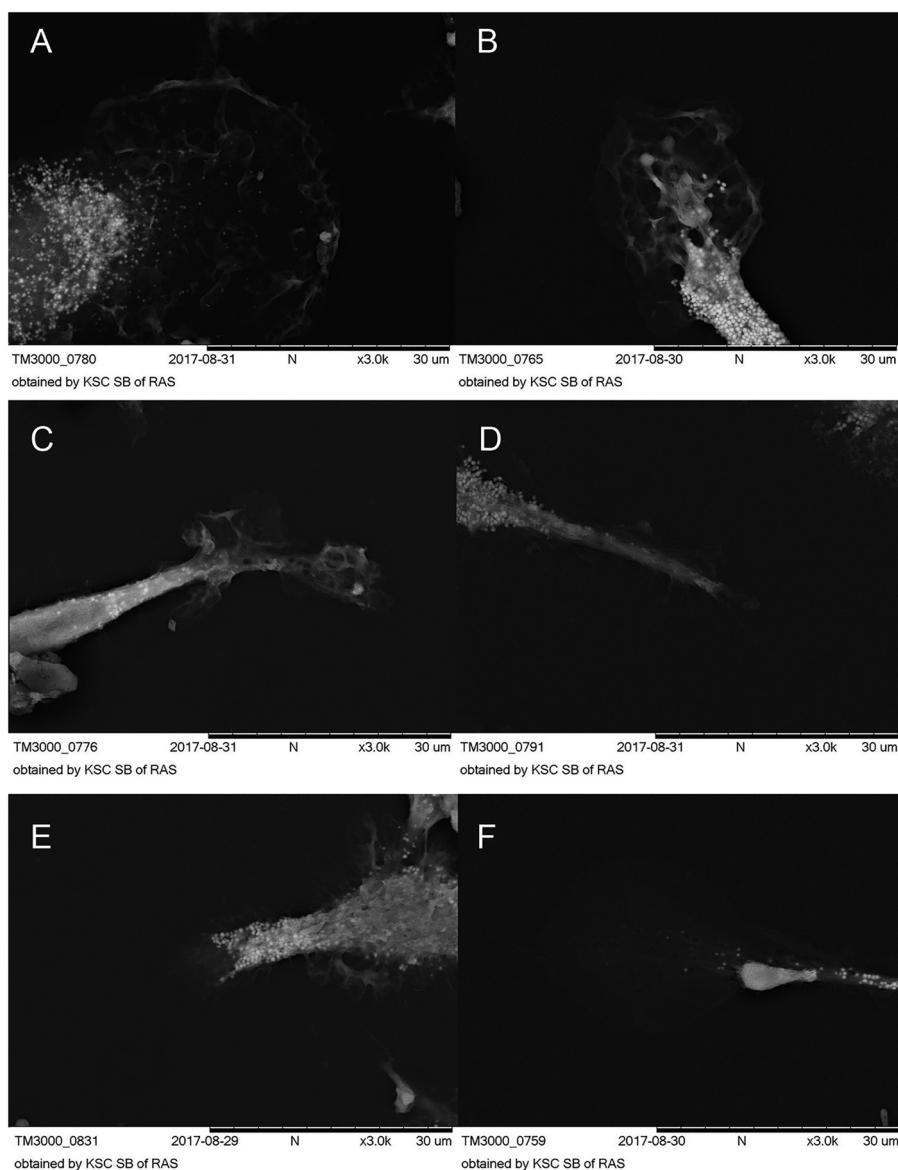
Fig. 6. Morphology of MPh lamelopodia on culture plastic. A – lamelopodia of the 1st morphological class cells. B, C, D, E, F – lamelopodia of the 2nd morphological class cells. F – a rounded paw lamelopodia typical for the morphotype of filamentous cells.

basic morphological classes (rounded and elongated cells) did not differ significantly from the variant before stent placement. Based on this it can be assumed that stent placement did not affect the number of mobile cells *in vitro*. But the relationship between the morphotypes in each morphological class changed radically after the stent was installed.

In the morphological class of elongated cells the number of filamentous and triangular cells decreased by 3.5 and 3 times respectively, and the number of rod-shaped cells increased by 1.7 times as compared with before stent placement (Table 3).

In the morphological class of rounded cells the percentage of the multinucleated cells did not change (in comparison with the variant before the stent was installed). But the ratio between the two morphotypes shifted strongly toward mononuclear cells: the number of multinucleated cells was 1.9 times lower than single nucleated cells (this ratio was 1.4 before stent placement).

The 3rd morphological class with indefinite morphology was not numerous when cultivated on plastics both before and after stenting and was low than 1% (Table 3) (Fig. 5a– d).

Complicated membranous relief in the periphery of round cells (Fig. 6a) and lamellipodia of cells of 2nd and 3d morphological classes

(Fig. 6b–e) were MPh characteristic on culture plastic. The lamellipodia of morphotypes of filamentous cells had the form of round-shaped pad flat leg (Fig. 6f).

3.2.1.3. MN-MPh culture on biopolymer scaffolds. The analysis of the surface of biopolymer scaffolds using SEM revealed a complex micro-nanoscale relief, which was formed during the drying of a polymer film.

The surface relief of the polymer samples varied depending on the monomeric composition. The relief of the scaffolds 1 and 4 was more "coarse" and loose with large deep pores (Fig. 7a, d). The surface relief of the scaffolds 2, 3 and 5 were more "delicate", resembling small ripples on water surface (Fig. 7b–e). The relief of the scaffold 5 was characterized by small numerous pores (Fig. 7e).

Morphological analysis of MPh on biopolymer scaffolds with various micro/nano relief revealed 3 main morphological classes, which were also observed during cell cultivation on culture plastics (Table 3). So, for example, a morphotype of spindle-shaped cells (the second morphological class) (Fig. 8a–e), which was observed on all samples was also encountered among the MPh on culture plastics (Fig. 4 c, d). Large round multinucleate cells (the 1st morphotype of the 1st
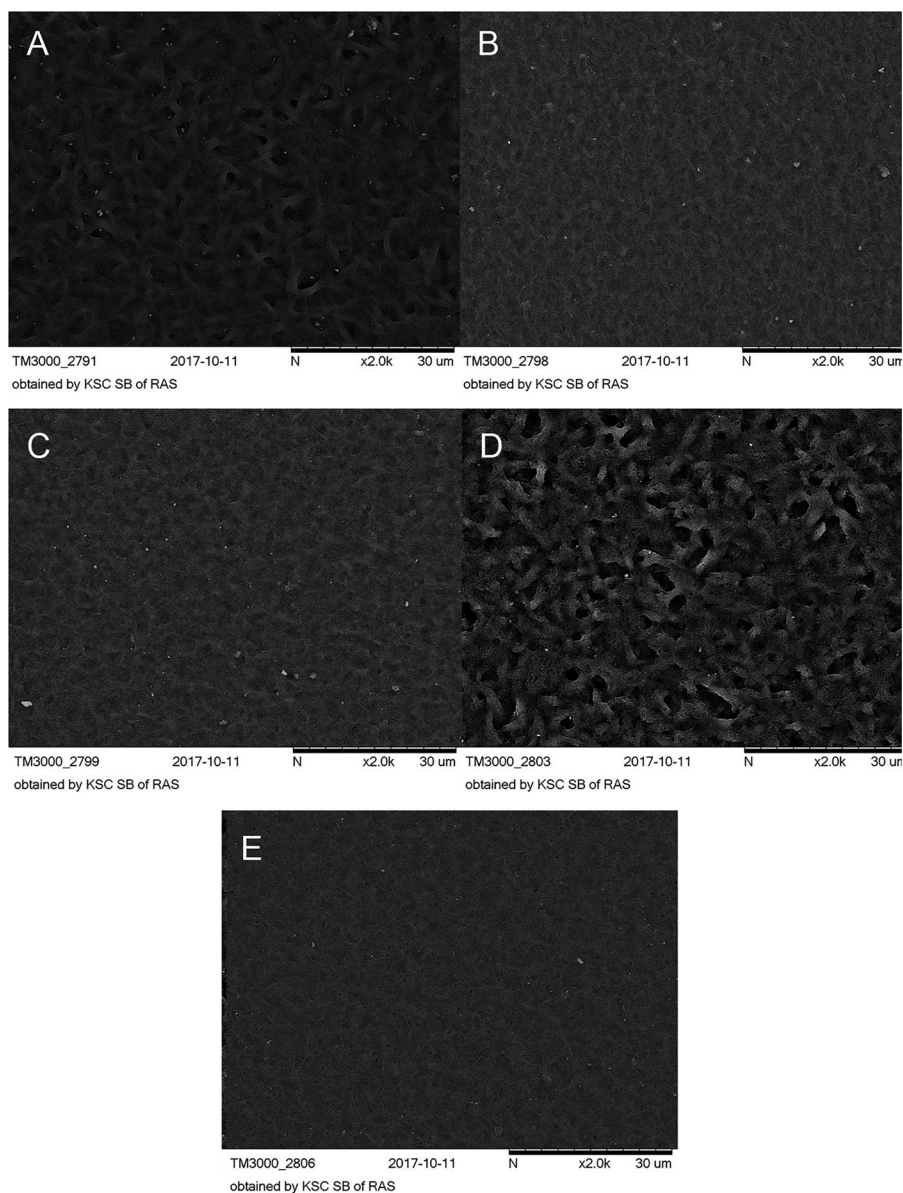
Fig. 7. Surface microrelief of the of biopolymer scaffolds of various composition (Table 1). A – scaffold 1; B – scaffold 2; C – scaffold 3; D – scaffold 4; E – scaffold 5.

morphological class) were observed on all biopolymer substrates, but on the substrate 5 these cells reached enormous sizes (Fig. 9a, b).

It should be noted, that the complex membranous relief along the periphery of rounded cells and lamelopodia of cells of the 2nd and 3rd morphological classes, which was characteristic for the results on the culture plastics, was significantly "simplified" on biopolymer scaffolds (Fig. 10a–e).

The same MPh morphotypes were detected on culture plastic and on biopolymer substrates, but the quantitative relationships between different morphotypes varied significantly depending on the characteristics of the micro/nano relief of the sample surface and on MN release option – before and after stent placement (Table 3).

On the basis of the morphological analysis several parameters were selected for an integral evaluation of the MPh morphology in different samples.

1. The ratio between the number of the 1st and 2nd morphological classes (the ratio between the number of rounded and elongated cellular forms), $K_{M1/M2}$ (Fig. 11).

This parameter varied significantly depending on the type of substrate and time of cell isolation, i.e whether isolated before or after stent

installation. For the cells, isolated before the stenting the parameter value decreased as follows: **Scaffold 2 (2.07)** > **Scaffold 3 (1.29)** > **Plastic (0.94)** > **Scaffold 5 (0.72)** > **Scaffold 4 (0.57)** > **Scaffold 1 (0.55).**

For the cells, isolated after the stent installation this parameter value decreased in an absolutely different way: **Scaffold 5 (1.44)** > **Plastic (1.22)** > **Scaffold 1 (0.87)** > **Scaffold 3 (0.71)** > **Scaffold 4 (0.24)** > **Scaffold 4 (0.24).**

It should be noted, that during cell cultivation on standard culture plastics the value of $K_{M1/M2}$ did not differ significantly in the culture variants before and after stent placement. For the culture on biopolymer scaffolds of different composition the value of $K_{M1/M2}$ was significantly different for variants before and after stent implantations. Moreover, the direction of $K_{M1/M2}$ variation was not the same for biopolymer scaffolds of different monomer composition. After stenting $K_{M1/M2}$ for the scaffolds 1 and 5 increased, for scaffolds 2, 3, and 4 – decreased if compared with the variant before stenting.

2. The ratio between the number of 2nd and 1st morphotypes in the 1st morphological class (the ratio between the number of mononuclear (MOC) and multinucleated (MUC) cells) $K_{MOC/MUC}$ (Fig. 12).
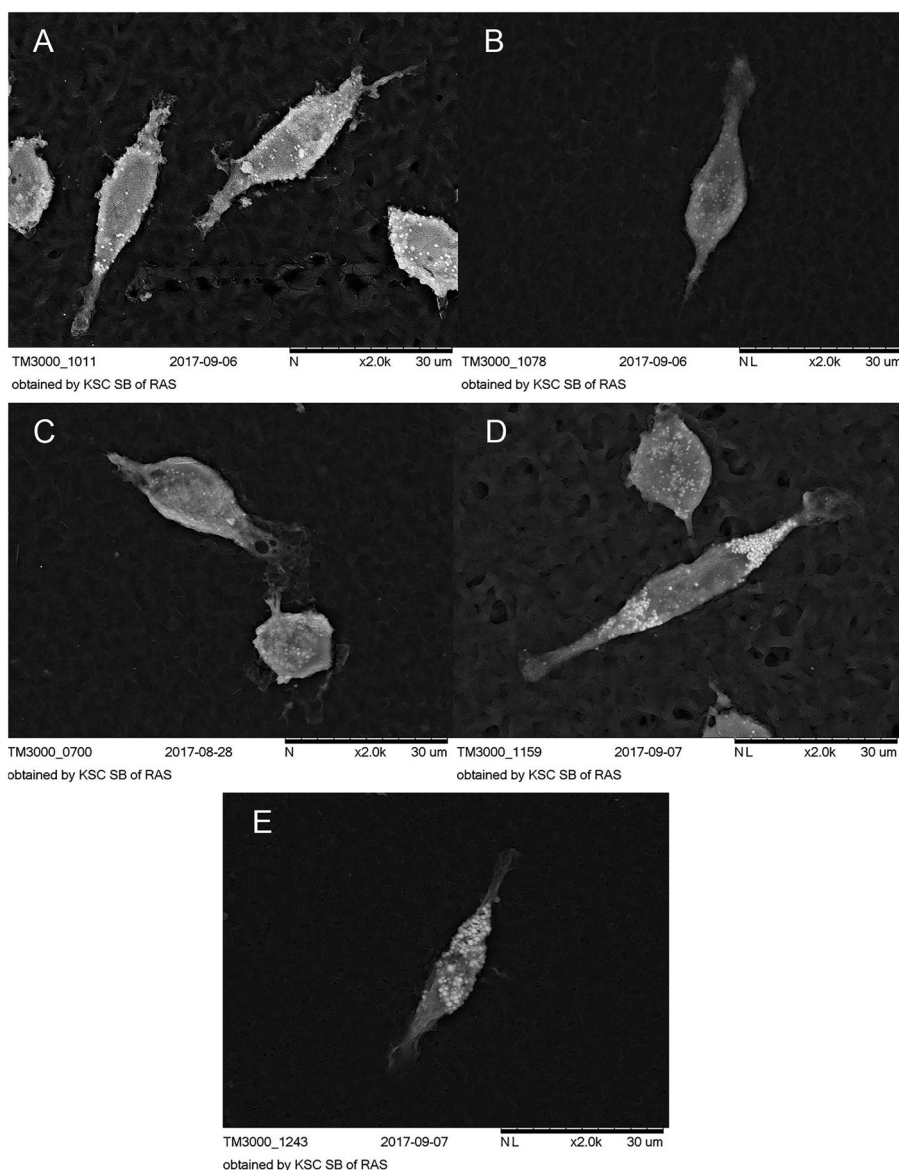
Fig. 8. Morphotype of spindle-shaped cells (2nd morphological class) on biopolymer scaffolds of different composition. A – scaffold 1; B – scaffold 2; C – scaffold 3; D – scaffold 4; E – scaffold 5.

Variability of this parameter was significantly higher than the $K_{MOC/MUC}$ parameter and depended on scaffold type and isolation time.

For the cells isolated before stent installation the value of $K_{MOC/MUC}$ decreased as follows: **Scaffold 2 (5.00) = Scaffold 3 (5.00) > Scaffold 5 (3.00) > Plastic (1.40) > Scaffold 4 (1.38) > Scaffold 1 (1.13).**

For the cells isolated after stent placement the value of this parameter decreased differently: **Scaffold 3 (9.00) > Scaffold 4 (2.50) > Scaffold 5 (2.30) > Plastic (1.90) > Scaffold 1 (1.12) > Scaffold 2 (0.82).**

The change direction in $K_{MOC/MUC}$ was not the same for biopolymer scaffolds of different composition. After stenting $K_{MOC/MUC}$ for culture plastic scaffolds 3 and 4 increased, for scaffolds 2 and 5 decreased, compared with the variant before stenting. For scaffolds 1 $K_{MOC/MUC}$ was the same before and after stenting.

For cultural plastic and various variants of biopolymer scaffolds specific ratio between the parameters $K_{M1/M2}$ and $K_{MOC/MUC}$ depended on cultivation variant before or after stenting. At the same time, it should be noted that the variability of the parameters of $K_{M1/M2}$ and $K_{MOC/MUC}$ was significantly higher for biopolymer scaffolds than for culture plastic. This allows us to consider such system as more promising for change assessment in MPh functional state *in vivo* (vascular bed), based on changes in differentiation processes of MN to MPh *in vitro*.

3.3. MTT reduction activity in MPh in various culture conditions

MTT test is based on the intracellular reduction of the water-soluble tetrazolium dye MTT into insoluble formazan with the participation of NAD(P)H-dependent oxidoreductases. Formazan formation depends on the availability of NAD(P)H and can serve as an integral measure of the activity of NAD(P)H production and the activity of NAD(P)H-dependent metabolic cycles [60,61]. NAD(P)H is known to play an important role in epigenetic and metabolic reprogramming of MPh (differentiation and polarization processes) [62–64]. In this connection, the activity of MTT reduction to formazan was determined under different culture conditions (Table 4).

It was shown that in case of MN isolation before stent installation MTT reduction activity on scaffolds 2 and 3 was 1.5 times less if compared to culture plastic. In case of MN isolation after the stent was
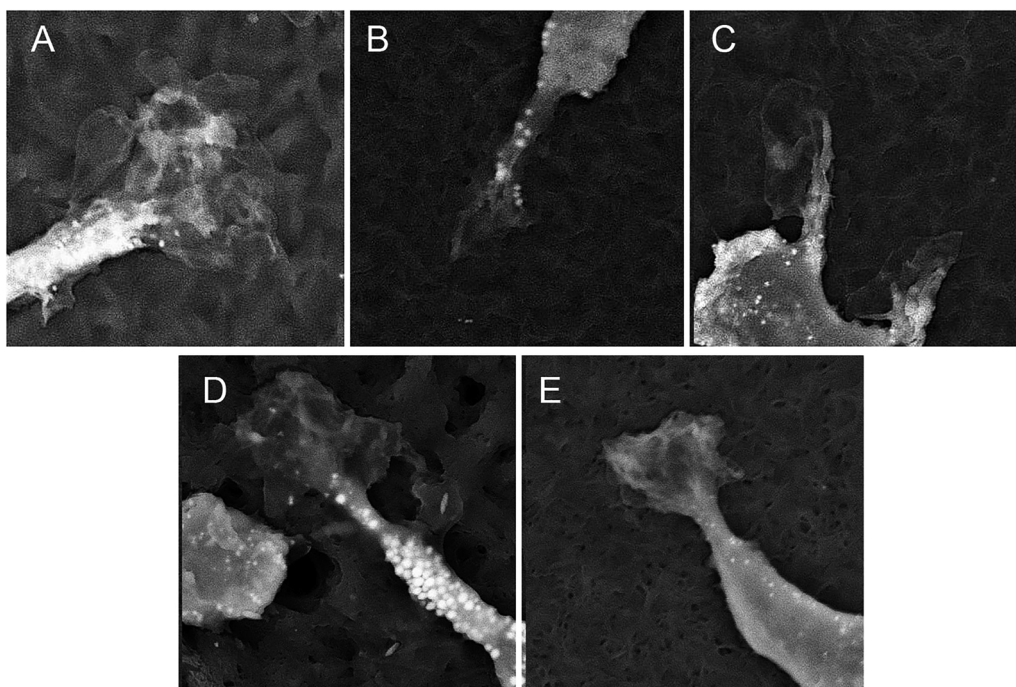
Fig. 9. Morphology of MPh lamelopodia on biopolymer scaffolds of different composition. A – scaffold 1; B – scaffold 2; C – scaffold 3; D – scaffold 4; E – scaffold 5.
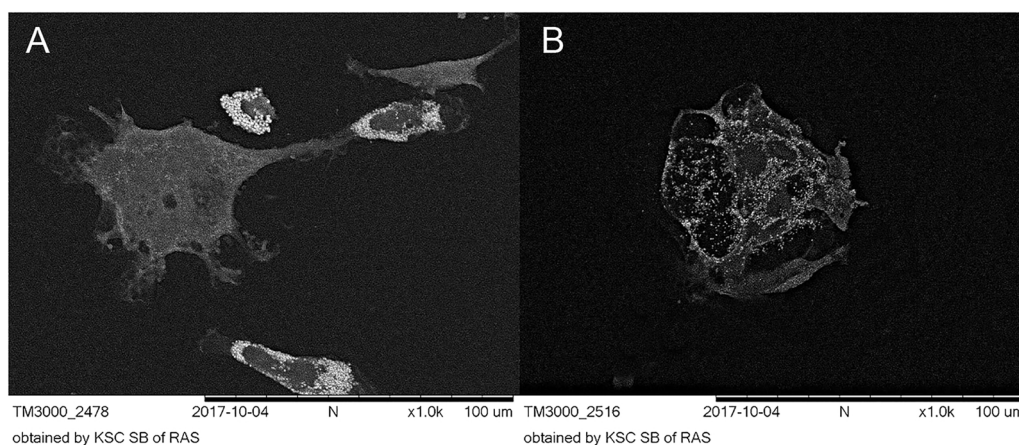
Fig. 10. Giant multinuclear cells on the biopolymer scaffold. A – neuron-like cell with lamelopodia; B – rounded cell with a lot of lipid droplets in the cytoplasm.

installed MTT reduction activity on the scaffold 4 was 1.5 times higher than that on culture plastic. These features were revealed for MTT reduction activity, expressed as a percentage of the control group (culture plastic) (Table 4). The analysis of the absolute values of optical density made it possible to reveal additional patterns (Table 4). After stent installation the MTT reduction activity on culture plastic and on the scaffold 1 decreased 1.7 times if compared with the corresponding values for the variant before stent placement (Table 4). There were no significant differences in the activity of MTT reduction in formazan between variants before and after stent placement on scaffolds 2, 3, 4, and 5.

It should be noted that at the cellular level the variability of morphotypes under different culture conditions was more significant than the variability of MTT reduction activity.

4. Discussion

Biopolymer P(3HB) is described as a completely non-toxic material and proposed to develop biodegradable implants or coatings, since in the process of biodegradation of this polymer toxic compounds for cells are not formed also. However, these characteristics are not sufficient for the prediction of the effectiveness of such biopolymers as scaffolds in *in vivo* systems.

We also took into account, that the physicomechanical properties of P(3HB) for biomedical applications are inferior to thousands of its copolymers, such as P(3HB/3HV), P(3HB/4HB), P(3HB/3HHx), and others, which accounts for the spectrum of the copolymer samples in this study.

In vivo and *in vitro*, contact interaction of the implant with the MPh triggers the processes of polarization (differentiation into M1/M2 MPh-phenotypes). *In vitro* studies indicate that polarization of MPh in the absence of specific inductors in the medium (interferon-γ and lipopolysaccharide for the induction of the M1-phenotype; interleukin-4 or interleukin-13 for the M2-phenotype) depends on the characteristics of the surface relief profile of the implant/contact material [18–23]. Under the conditions of co-cultivation of MPh and various types of progenitor cells *in vitro*, the effects of surface relief on the processes of differentiation and proliferation of progenitor cells are realized through the processes of polarization of MPh [22,19–23]. Thus, activity of osteogenic differentiation of mice bone marrow mesenchymal stem cells
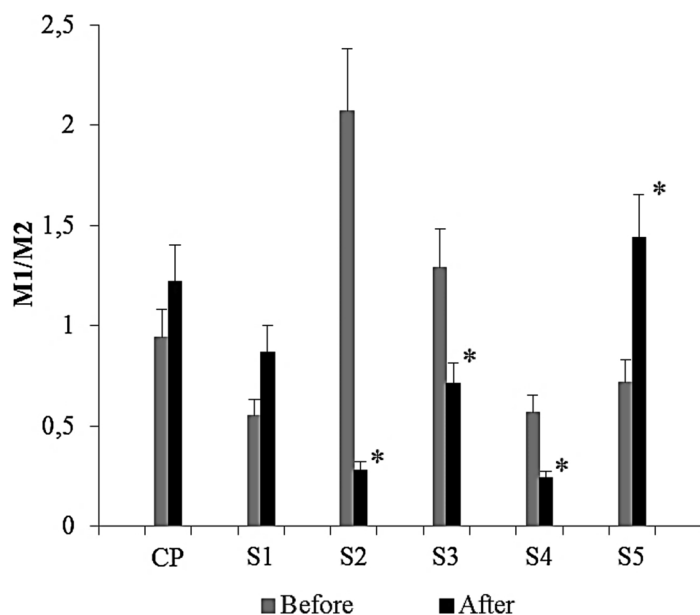
Fig. 11. The ratio between the cell number of the 1st and the 2nd morphological classes (M1/M2-phenotypes) on the 6th day on culture plastic and biopolymer scaffolds before (Before) and after (After) stenting. M1 – rounded cells, M2 – elongated cells. Abscissae axis: CP – culture plastic; S1 – scaffold 1; S2 – scaffold 2; S3 – scaffold 3; S4 – scaffold 4; S5 – scaffold 5. An asterisk indicates the cases where the value after the stent installation (After) was significantly different from the value before the stent installation (Before) ($p \leq 0.05$).
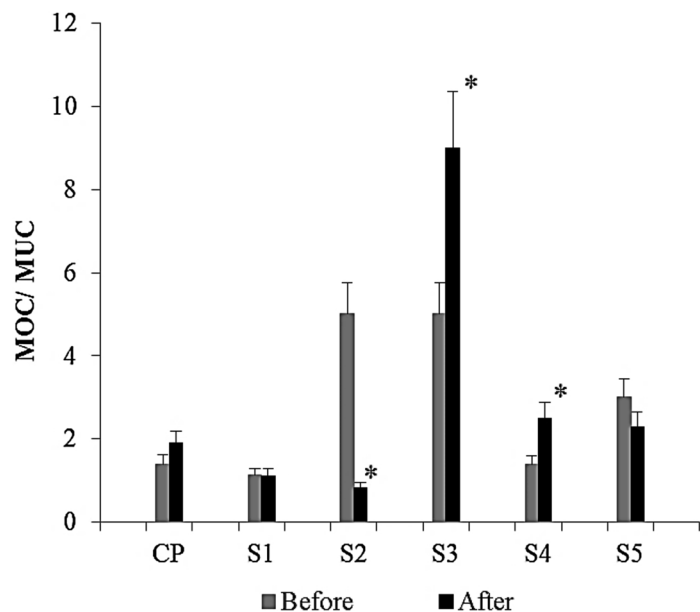
Fig. 12. The ratio between the rounded mononuclear cells (MOC) and rounded multinuclear cells (MUC) (1st morphological class) on the 6th day on culture plastic and biopolymer scaffolds before and after stenting. Abscissae axis: CP – culture plastic; S1 – scaffold 1; S2 – scaffold 2; S3 – scaffold 3; S4 – scaffold 4; S5 – scaffold 5. An asterisk indicates the cases where the value after the stent installation (After) was significantly different from the value before the stent installation (Before) ($p \leq 0.05$).

on nanostructured titanium plates was highest on the samples with variants of reliefs, what inducted M2-polarization of MPh [18]. On topographycal variants of titanium surfaces, that induced M1 polarization of MPh, inhibition of fibroblast proliferation was observed [19].

In vitro polarization of MPh is accompanied by changes in cell morphology. M2-MPh is characterized by a longitudinal extended, elongated cell shape. It was shown that surface reliefs, consists from ordered grooves contributed to the formation of elongated morphological forms of MPh, which began to express markers of the M2-phenotype, without introducing of specific inductors into the medium [65,66]. This allows the use of morphological analysis to determine the M1/M2 ratio of MPh-phenotypes on various surface relief variants and to predict the "toxicity" of surface nano-topography *in vitro*.

The reason for such a diversity of MPh morphotypes *in vitro* may be the heterogeneity of monocytes circulating in the blood *in vivo* [67–70]. By the nature of expression of surface antigens, three subpopulations of circulating MN are isolated: CD14^{++}CD16^{-}-classic MN1, CD14^{++}CD16^{+}-interim MN2, and CD14^{+}CD16^{++}-Mn3, non-classical. But it is possible to "divide" MN into various subpopulations using

other surface antigens [71].

Subpopulations are characterized by differential expression of the genes that determine their specific functions and implications for physiological and pathogenic processes. [72,73] Specific MN subpopulations control the structural and functional integrity of the vascular endothelium, activity of infiltration of neutrophils in tissues. Certain MN subpopulations leave the vascular bed and patrol the extracellular space of various organs and tissues and return back to the bloodstream (possibly in another morphological and functional status state) [72–77]. For such pathology as atherosclerosis, the active yield of MPh-foam cells from the body of an atherosclerotic plaque is considered as one of the approaches to targeting this disease. It is possible, that different MN subpopulations give rise to specific MPh subpopulations and dendritic cells in tissues and organs [78].

MPh subpopulation is a labile system, the number and functional activity of which can vary considerably in terms of physiological norm and pathogenesis [79]. There is reason to believe that subpopulations of circulating MN are different stages of cellular differentiation [80], which may be modified under the influence of various factors.

Table 4

MTT assay: activity of MTT reduction to formazan in various cultivation conditions. MN were isolated from the patient's blood before the stent was installed (Before) and after the stent was installed (After). MN were cultured on culture plastic (CP) and on the biopolymer scaffolds of various compositions (S1, S2, S3, S4, S5) in 96-well culture plates (10^5 cells/well) in DMEM medium with 10% fetal serum in a CO_2 incubator. After 6 days of culture the activity of MTT reduction to formazan was determined. MTT assay results were presented in % of control (culture plastic, 100%). The activity of MTT reduction is presented as an optical density at $\lambda = 550$ nm in parentheses, under percentages.

MN isolation	Scaffolds					
	S1	S2	S3	S4	S5	CP
Before	116% (0.405)	63% (0.220)*	68% (0.237)*	98% (0.338)	82% (0.284)	100% (0.348)
After	118% (0.232)#	92% (0.180)	119% (0.233)	149% (0.293)*	109% (0.214)	100% (0.196)#

Asterisk * indicates the values significantly different from the values for culture plastic (CP) ($p \le 0.05$) for each variant of MN isolation (before or after stenting). The # icon indicates the values for the MN isolated after the stent installation (After) significantly different from the values for the MN isolated before the stent installation (Before) ($p \le 0.05$).

Stent placement is a surgical procedure, associated with a relatively small loss of blood, but with the tangible intervention into vessel. Even this insignificant blood loss can provoke the release of a fresh portion of MN from the bone marrow. On the other hand, an X-ray contrast substance is introduced to conduct stenting in the bloodstream, which can affect the functional state of circulating MN. Finally, being a fairly rigid mechanical structure, the stent in the delivering system can damage the endothelium of intact parts of the vascular wall, endothelium in the zone of plaque and the body of the plaque itself. As a result, in focused zone the local gradient of cell degradation products may accumulate. These are chemical signals which can affect the zone passing through the stent MN. Ultimately, by the time of resampling of blood from a patient in a day after the stent placement circulating MN (the ratio of different subpopulations of functional phenotypes, *i.e.*, structural and functional heterogeneity) may differ significantly from MN isolated from the patient's blood before the stent placement.

We must assume that the structural and functional heterogeneity of MN *in vivo* determines the characteristics of interaction with cell anchorage and morphotypes diversity in cell culture scaffolds *in vitro*. It is known, that changes in the morphology of cells, nuclei and cell organelles may trigger signaling system of metabolic and epigenetic reprogramming in cells (mechanochemical signaling) [55,56,80–83]. And in this connection the analysis of cellular morphotypes can be useful at the stage of screening cultural substrates of various compositions for the presence of "reprogramming" activity.

It was shown, that the functional M1-M2 polarization in MPh *in vitro* is associated with cell morphology: rounded MPh fall into the M1-phenotype (proinflammatory MPh), MPh with the elongate shape – to the M2 phenotype (MPh involved in repair processes) [84,85]. Based on the morphological characteristics (the ratio of the number of 1st and 2d morphological classes, rounded and elongated cells, Table 3), we can conclude, that before the stent installation in the process of MPh differentiation and polarization on culture plastic the ratio of cell populations with M1 and M2 phenotype was the same (M1/M2 = 0.94). After stent placement, the ratio of M1 and M2 phenotypes did not change significantly (M1/M2 = 1.22), but it became slightly higher.

Among the rounded cells (the 1st morphological class), large multinuclear MPh were observed as the fusion result of several mononuclear cells (Fig. 2 a, b; 9). The process of cell fusion is a cellular reaction of MPh, which is triggered, in particular, by the interaction with the implant material (giant multinuclear cells *in vivo*) [86,87]. It is assumed, that the interaction of MPh with highly curved surfaces triggers the processes of cell fusion (possibly *via* the system of

mechanochemical signaling). One such an example is multinuclear osteoclasts, MPh of bone tissue, "working" with such surface type. It is assumed, that the giant multinuclear MPh may also be subjected to the M1-M2-polarization and their round shape is not always indicative of M1 phenotype [88].

Before and after stent placement the total number of multinuclear MPh on culture plastics was the same (19%), *i.e.* the activity of the fusion reaction of mononuclear MPh on the culture plastic surface after the stent installation procedure did not change. However, the ratio between multinuclear and mononuclear MPh after stent placement shifted toward mononuclear cells: the number of multinuclear cells was 1.9 times less, than the number of mononuclear cells. Before the stent installation this ratio was 1.4 (Fig. 12).

Statistically significant changes in the ratio of the number of M1 and M2 phenotypes, rounded and elongated cells, *i.e.* changes in the direction of the processes of MPh polarization on culture plastics before and after stent placement were not observed. However, this may be not due to the absence of changes in the MN population, and accordingly, to the differentiation and polarization processes of MPh after stent placement, but to the peculiarities of culture plastic, that do not allow to reveal these changes at the morphological level.

This assumption is confirmed by the morphological analysis of MPh before and after stent placement during cultivation on biopolymer scaffolds with different composition: the stent installation procedure has a significant effect on functional phenotypes of circulating MN *in vivo* and resulted in significantly modified differentiation and polarization of MPh *in vitro*.

Quantitative changes in the ratio of different MPh morphotypes before and after stenting were expressed to a much greater extent on biopolymer scaffolds than on culture plastics (Fig.13a–g). Based on changes in the number of M1-M2 phenotypes (Fig. 11) we can say that the biopolymer scaffolds may affect the processes of polarization of MPh *in vitro* and this influence is determined by the monomer composition and micro/nano relief of the scaffolds. And the polarization direction of MPh *in vitro* at the same biopolymer scaffolds also depends on the initial functional state of MN *in vivo* at the time of the isolation of these cells (Fig. 11). It can be assumed, that in 24 h after the stent installation new structural and functional phenotypes were formed in the MN population of the vascular bed. It determines the development of new "relationships" of cells with the biopolymer scaffolds and, accordingly, specific variants of differentiation and polarization of MPh *in vitro*. This is important fact not only for screening in the systems *in vitro*. Stenting as the surgical procedure and the foreign body can provoke 'aggressive' behavior of the MN and the formation of "hot points" in the zones of stenting, which may disturb the process of re-endothelization of the stent to activate the proliferation of smooth muscle cells and ultimately lead to restenosis.

Along with the variability of MPh polarization processes, one should note the variability of the number of multinuclear MPh forms. The number of these cells also depends on the composition of the biopolymer scaffolds and on the variant of obtaining MN – before or after the stenting. So, on the sample scaffold 5 the number of multinuclear forms of MPh increased after stenting, and on scaffolds 3 and 4 – it decreased if compared with the variant before stenting. In substrates 1 and 2 and in control on culture plastics, the number of multinuclear MPh before and after stenting was the same (Table 3, Fig. 12). The surface topography of implants affects not only the processes of phenotypic differentiation of the MPh, but also determines the activity of the confluence of the MPh and formation of multinucleated giant cells and giant foreign body cells [89].

Formation of multinuclear cells is the cell adaptation, aimed at improving the efficiency of degradation of foreign materials with large radius of curvature [88]. It can be assumed, that the different number of multinuclear MPh under different cultivation conditions can determine the biodegradability of biopolymers, used for the production of experimental scaffolds. And the dynamics of biodegradation is determined
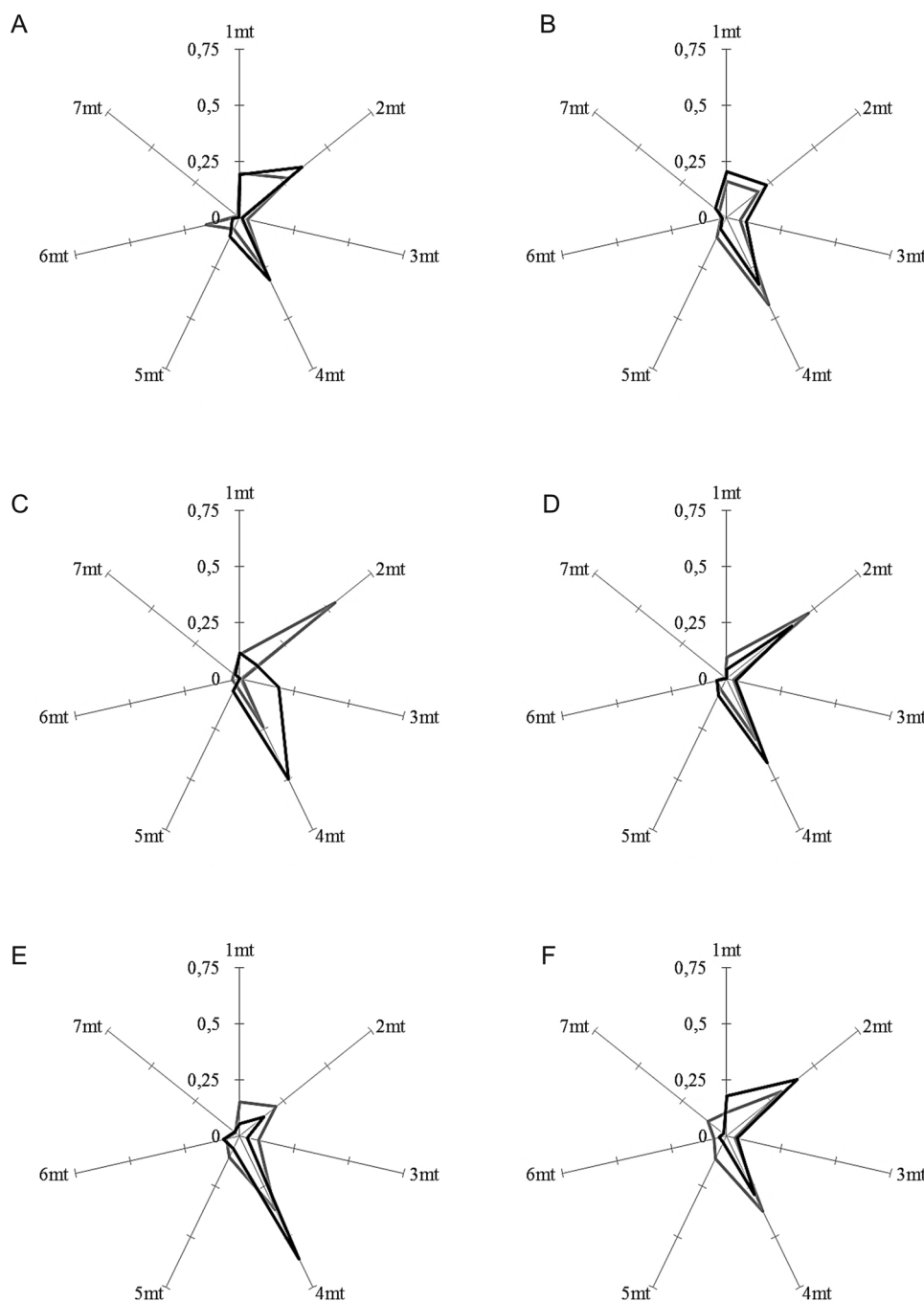
Fig. 13. The ratio of different morphotypes (mt) on the 6th day on culture plastic and biopolymer scaffolds of different composition before (Before) and after (After) stent installation. A – culture plastic; B – scaffold 1; C – scaffold 2; D – scaffold 3; E – scaffold 4; F – scaffold 5. 1 mt – the morphotype of multinucleated cells; 2 mt – morphotype of rounded single nucleated cells; 3 mt – morphotype of filamentous cells; 4 mt – morphotype of spindle-shaped cells; 5 mt – morphotype rod-shaped cells; 6 mt – morphotype of "triangular" cells; 7 mt – morphotype of a cells with unusual morphology.

not only by biopolymer properties, but also by the variability of the processes of differentiation and polarization of MPh.

As already mentioned, it is customary to refer elongated cells to M2-MPh. In this morphological class various quantitative relationships between these four different morphotypes were formed on different biopolymer scaffolds before and after stenting. In general, the morphology of these cells indicates their mobility and active movement along the substrate. It is possible, that these are different subpopulations of MPh with different molecular "ways" of locomotion. Different types of locomotor behavior were demonstrated on a monolayer of endothelial cells *in vitro* for different MN subpopulations (classic $CD14^{++}CD16^{-}$, intermediate $CD14^{++}CD16^{+}$, and not-classical

$CD14^{+}CD16^{++}$). These differences in locomotor behavior of MN subpopulations were associated with different adhesion molecules [90].

It is possible, that the variability in the number of mobile morphotypes of MPh can also be related to the features of substrate relief. The smooth surface of the culture plastic and the complex relief of the biopolymer scaffolds determine different activity of the cell adhesion processes, locomotion machinery and cell morphology, as a result. Moreover, it should be noted, that not only the relief structure determines the locomotion machinery, but the features of the functional phenotype of MPh can form different types of locomotor behavior of cells on the same biopolymer scaffold. Thus, on the biopolymer scaffold 2 after the stent was installed, the number of the morphotype of the

filamentous cells increased 18-fold, compared with the variant before the stent was installed.

MPh polarization, along with morphological changes, is associated with metabolic reprogramming. The pentose-phosphate pathway (or hexose-monophosphate shunt) is the key metabolic pathway which the direction of MPh polarization depends on. Hexose monophosphate shunt is the main metabolic pathway, generating NADPH. The M1-polarization process is associated with the direction of the glucose flow into the hexose-monophosphate shunt and the increase in NADPH production [62, 91]. NADPH as an energy equivalent uses various oxidoreductases, producing reactive oxygen species, which are included in the processes of epigenetic reprogramming of MPh [92]. In M2-MPh glucose flux in the hexose monophosphate shunt is limited, and NADPH synthesis activity drops sharply [91].

i.e., in the first approximation, we can assume that the high level of NADPH production in M1-MPh can identify and recover a high activity of MTT reduction in formazan by NADPH-oxidoreductases. The variability of MTT reduction activity in formazan can depend on the ratio of M1/M2 phenotypes. However, the correlation analysis did not reveal reliable correlations between these two parameters.

In general, the variability of MTT reduction activity was insignificant for various cultivation options (compared to the variability of cellular morphotypes). This integral parameter of the metabolic activity of cells is not demonstrative for the primary screening of the reprogramming activity of biopolymer scaffolds.

The results show the effectiveness of the primary screening reprogramming activity of biopolymers (as potential materials for vascular stents) on the basis of morphological analysis of MPh-culture *in vitro*. Based on the obtained results, samples of biopolymers will be selected for further study of the cellular polarization processes of MPh with the use of specific markers.

5. Conclusion

We determined 3 morphological classes of MN-MPh during the cultivation of cells of patients with atherosclerosis:

1st morphological class – rounded cells (M1-phenotype) which have 2 morphotypes: mononuclear and multinuclear cells;

The 2nd morphological class is elongated cells (M2 phenotype) which have 4 morphotypes: filiform, spindle-shaped, rod-shaped and triangular cells;

3rd morphological class – cells of unusual shape.

The proportion of morphotypes in the MPh cell population depends on the profile of the contact surface of the sample of PHAs and on its monomer composition. The procedure of stenting also affects the ratio of MPh morphotypes. The number of multinuclear cells on PHAs-samples of different compositions may indicate the activity of polymers biodegradation, similarly to the process of formation of giant cells of foreign bodies *in vivo*.

The obtained results demonstrate the dependence of the biological activity of biodegradable polymer scaffolds of different compositions not only on the specificity of the micro/nano relief of their surface, but also on the features of the initial structural-functional state of MN blood population in patients before and after the intervention. Specific ratios of MPh morphotypes adequately reflect the interaction of surface relief and functional phenotype of cells *in vitro,* and this ability may be useful for screening of «toxicity» of surface reliefs of biomaterials for cardiovascular surgery and stents of new age, and for effective monitoring of molecular-cellular events in the area of intervention in patients after procedure. The surface profile of the material affects the polarization processes and has the ability to trigger the systems of mechanochemical signaling and subsequent reprogramming of metabolism, reorganization of the cytoskeleton and cell epigenome.

Conflicts of interest

The authors declare no conflict of interest.

References

[1] A.A. Artyukhov, M.I. Shtilman, A.N. Kuskov, L.I. Pashkova, A. Tsatsakis, A.K. Rizos, Polyvinyl alcohol cross-linked macroporous polymeric hydrogels: structure formation and regularity investigation, J. Non. Solids 357 (2011) 700–706.

[2] Z. Pan, J. Ding, Poly(lactide-co-glycolide) porous scaffolds for tissue engineering and regenerative medicine, Interface Focus 2 (2012) 366–377.

[3] Z. Piperigkou, K. Karamanou, A.B. Engin, C. Gialeli, A.O. Docea, D.H. Vynios, M.S.G. Pavão, K.S. Golokhvast, M.I. Shtilman, A. Argiris, E. Shishatskaya, A.M. Tsatsakis, Emerging aspects of nanotoxicology in health and disease: from agriculture and food sector to cancer therapeutics, Food Chem. Toxicol. 91 (2016) 42–57.

[4] J.P. Mazzoccoli, D.L. Feke, H. Baskaran, P.N. Pintauro, Mechanical and cell viability properties of crosslinked low- and high-molecular weight poly(ethylene glycol) diacrylate blends, J. Biomed. Mater. Res. A 93 (2009) 558–566.

[5] S.P. Zustiak, J.B. Leach, Hydrolytically degradable poly(ethylene glycol) hydrogel scaffolds with tunable degradation and mechanical properties, Biomacromolecules 11 (2010) 1348–1357.

[6] H.K. Makadia, S.J. Siegel, Poly lactic-co-glycolic acid (PLGA) as biodegradable controlled drug delivery carrier, Polymers 3 (2011) 1377–1397.

[7] T. Zhang, L.Q. Wan, Z. Xiong, A. Marsano, R. Maidhof, M. Park, Y. Yan, G. Vunjak-Novakovic, Channelled scaffolds for engineering myocardium with mechanical stimulation, J. Tissue Eng. Regen. Med. 6 (2011) 748–756.

[8] Y. Li, H. Meng, Y. Liu, B.P. Lee, Fibrin gel as an injectable biodegradable scaffold and cell carrier for tissue engineering, Transfus. Apher. Sci. (2015) 1–10, https://doi.org/10.1155/2015/685690.

[9] A.N. Kuskov, P.P. Kulikov, M.I. Shtilman, V.N. Rakitskii, A. Tsatsakis, Amphiphilic poly-N-vynilpyrrolidone nanoparticles: cytotoxicity and acute toxicity study, Food Chem. Toxicol. 96 (2016) 273–279.

[10] A.L. Luss, P.P. Kulikov, S.B. Romme, C.L. Andersen, C.P. Pennisi, A.O. Docea, A.N. Kuskov, K. Velonia, Y.O. Mezhuev, M.I. Shtilman, A.M. Tsatsakis, L. Gurevich, Nanosized carriers based on amphiphilic poly-N-vinyl-2-pyrrolidone for intranuclear drug delivery, Nanomedicine 13 (2018) 703–715.

[11] A. Hudita, B. Galateanu, S. Dinescu, M. Costache, A. Dinischiotu, C. Negrei, M. Stan, A. Tsatsakis, D. Nikitovic, D. Lupuliasa, A. Balanescu, In Vitro Effects of Cetylated Fatty Acids Mixture From Celadrin on Chondrogenesis and Inflammation With Impact on Osteoarthritis, CART, 2018, https://doi.org/10.1177/1947603518775798 194760351877579.

[12] F.O. Martinez, L. Helming, S. Gordon, Alternative activation of macrophages: an immunologic functional perspective, Annu. Rev. Immunol. 27 (2009) 451–483.

[13] D.M. Mosser, J.P. Edwards, Exploring the full spectrum of macrophage activation, Nat. Rev. Immunol. 8 (2008) 958–969.

[14] J. Wang, F. Meng, W. Song, J. Jin, Q. Ma, D. Fei, L. Fang, L. Chen, Q. Wang, Y. Zhang, Nanostructured titanium regulates osseointegration via influencing macrophage polarization in the osteogenic environment, Int. J. Nanomed. 13 (2018) 4029–4043.

[15] X. Wang, Y. Wang, D.D. Bosshardt, R.J. Miron, Y. Zhang, The role of macrophage polarization on fibroblast behavior – an *in vitro* investigation on titanium surfaces, Clin. Oral Investig. 22 (2018) 847–857.

[16] D. Kosoff, J. Yu, V. Suresh, D.J. Beebe, J.M. Lang, Surface topography and hydrophilicity regulate macrophage phenotype in milled microfluidic systems, Lab Chip 18 (2018) 3011–3017.

[17] M. Shayan, J. Padmanabhan, A.H. Morris, B. Cheung, R. Smith, J. Schroers, T.R. Kyriakides, Nanopatterned bulk metallic glass-based biomaterials modulate macrophage polarization, Acta Biomater. 75 (2018) 427–438.

[18] K. Li, D. Hu, Y. Xie, L. Huang, X. Zheng, Sr-doped nanowire modification of Ca-Si-based coatings for improved osteogenic activities and reduced inflammatory reactions, Nanotechnology 29 (2018) 084001, , https://doi.org/10.1088/1361-6528/aaa2b4.

[19] Z. Zhang, Y. Xie, H. Pan, L. Huang, X. Zheng, Influence of patterned titanium coatings on polarization of macrophage and osteogenic differentiation of bone marrow stem cells, J. Biomater. Appl. 32 (2018) 977–986.

[20] M. Le Borgne, G. Caligiuri, A. Nicoletti, Once upon a time: the adaptive immune response in atherosclerosis – a fairy tale no more, Mol. Med. 21 (2015) 8–13.

[21] S. Zaina, G. Lund, Connecting the dots between fatty acids, mitochondrial function, and DNA methylation in atherosclerosis, Curr. Atheroscler. Rep. 19 (2017) 36, https://doi.org/10.1007/s11883-017-0673-y.

[22] X. Yang, Y. Li, X. Ren, X. Zhang, D. Hu, Y. Gao, Y. Xing, H. Shang, Oxidative stress-mediated atherosclerosis: mechanisms and therapies, Front. Physiol. 8 (2017) 600, https://doi.org/10.3389/fphys.2017.00600.

[23] A. Zmysłowski, A. Szterk, Current knowledge on the mechanism of atherosclerosis and pro-atherosclerotic properties of oxysterols, Lipids Health Dis. 16 (2017) 188, https://doi.org/10.1186/s12944-017-0579-2.

[27] T. Block, A. El-Osta, Epigenetic programming, early life nutrition and the risk of metabolic disease, Atherosclerosis 266 (2017) 31–40.

[28] S.J. Jia, K.Q. Gao, M. Zhao, Epigenetic regulation in monocyte/macrophage: a key player during atherosclerosis, Cardiovasc. Ther. 3 (2017), https://doi.org/10.1111/1755-5922.12262.

[29] N. Khyzha, A. Alizada, M.D. Wilson, J.E. Fish, Epigenetics of atherosclerosis: emerging mechanisms and methods, Trends Mol. Med. 23 (2017) 332–347.

[30] F.D. Kolodgie, K. Yahagi, H. Mori, M.E. Romero, H.H. Trout, A.V. Finn, R. Virmani, High-risk carotid plaque: lessons learned from histopathology, Semin. Vasc. Surg. 30 (2017) 31–43.

[31] G.F. Bories, N. Leitinger, Macrophage metabolism in atherosclerosis, FEBS Lett. 591 (2017) 3042–3060.

[32] L. Panh, O. Lairez, J.B. Ruidavets, M. Galinier, D. Carrié, J. Ferrières, Coronary artery calcification: from crystal to plaque rupture, Arch. Cardiovasc. Dis. 110 (2017) 550–561.

[33] M. Kowara, A. Cudnoch-Jedrzejewska, G. Opolski, P. Wlodarski, MicroRNA regulation of extracellular matrix components in the process of atherosclerotic plaque destabilization, Clin. Exp. Pharmacol. Physiol. 44 (2017) 711–718.

[34] M.F. Brancati, F. Burzotta, C. Trani, O. Leonzi, C. Cuccia, F. Crea, Coronary stents and vascular response to implantation: literature review, Pragmat. Obs. Res. 8 (2017) 137–148.

[35] K. Nakamura, J.H. Keating, E.R. Edelman, Pathology of endovascular stents, Interv. Cardiol. Clin. 5 (2016) 391–403.

[36] J. Ng, C.V. Bourantas, R. Torii, H.Y. Ang, E. Tenekecioqlu, P.W. Serruys, N. Foin, Local hemodynamic forces after stenting: implications on restenosis and thrombosis, Arterioscler. Thromb. Vasc. Biol. 37 (2017) 2231–2242.

[37] R.S. Stankevich, A. Gudima, V.D. Filimonov, H. Klüter, E.M. Mamontova, S.I. Tverdokhlebov, J. Kzhyshkowska, Surface modification of biomaterials based on high-molecular polylactic acid and their effect on inflammatory reactions of primary human monocyte-derived macrophages: perspective for personalized therapy, Mater. Sci. Eng. C Mater. Biol. Appl. 51 (2015) 117–126.

[38] J. Kzhyshkowska, A. Gudima, V. Riabov, C. Dollinger, P. Lavalle, N.E. Vrana, Macrophage responses to implants: prospects for personalized medicine, J. Leukoc. Biol. 98 (2015) 953–962.

[39] C.D. Mills, M1 and M2 macrophages: oracles of health and disease, Crit. Rev. Immunol. 32 (2012) 463–488.

[40] M. Peled, E.A. Fisher, Dynamic aspects of macrophage polarization during atherosclerosis progression and regression, Front. Immunol. 5 (2014) 579, https://doi.org/10.3389/fimmu.2014.00579.

[41] A. Gombozhapova, Y. Rogovskaya, V. Shurupov, M. Rebenkova, J. Kzhyshkowska, S.V. Popov, R.S. Karpov, V. Ryabov, Macrophage activation and polarization in post-infarction cardiac remodeling, J. Biomed. Sci. 24 (2017) 13, https://doi.org/10.1186/s12929-017-0322-3.

[42] D. Zhou, C. Huang, Z. Lin, S. Zhan, L. Kong, C. Fang, J. Li, Macrophage polarization and function with emphasis on the evolving roles of coordinated regulation of cellular signaling pathways, Cell. Signal. 26 (2014) 192–197.

[43] D.A. Hume, The many alternative faces of macrophage activation, Front. Immunol. 6 (2015) 370, https://doi.org/10.3389/fimmu.2015.00370.

[44] L. Gaffney, P. Warren, E.A. Wrona, M.B. Fisher, D.O. Freytes, Macrophages' role in tissue disease and regeneration, Results Probl. Cell Differ. 62 (2017) 245–271.

[45] G.S. Boersema, N. Grotenhuis, Y. Bayon, J.F. Lange, Y.M. Bastiaansen-Jenniskens, The effect of biomaterials used for tissue regeneration purposes on polarization of macrophages, Bioresor. Open Access. 5 (2016) 6–14.

[46] J.L. Gallop, A. Walrant, L.C. Cantley, M.W. Kirschner, Phosphoinositides and membrane curvature switch the mode of actin polymerization via selective recruitment of toca-1 and Snx9, Proc. Natl. Acad. Sci. U. S. A. 110 (2013) 7193–7198.

[47] I.K. Jarsch, F. Daste, J.L. Gallop, Membrane curvature in cell biology: an integration of molecular mechanisms, J. Cell Biol. 214 (2016) 3753–3787.

[48] A.A. Bridges, M.S. Jentzsch, P.W. Oakes, P. Occhipinti, A.S. Gladfelter, Micron-scale plasma membrane curvature is recognized by the septin cytoskeleton, J. Cell Biol. 213 (2016) 23–32.

[49] K.R. Rosholm, N. Leijnse, A. Mantsiou, V. Tkach, S.L. Pedersen, V.F. Wirth, L.B. Oddershede, K.J. Jensen, K.L. Martinez, N.S. Hatzakis, P.M. Bendix, A. Callan-Jones, D. Stamou, Membrane curvature regulates ligand-specific membrane sorting of GPCRs in living cells, Nat. Chem. Biol. 13 (2017) 724–729.

[50] F. Daste, A. Walrant, M.R. Holst, J.R. Gadsby, J. Mason, J.E. Lee, D. Brook, M. Mettlen, E. Larsson, S.F. Lee, R. Lundmark, J.L. Gallop, Control of actin polymerization via the coincidence of phosphoinositides and high membranecurvature, J. Cell Biol. 216 (2017) 3745–3765.

[51] M. Galic, I. Begemann, A. Viplav, M. Matis, Force-control at cellular membranes, Bioarchitecture 4 (2014) 164–168.

[52] M. Emmert, P. Witzel, D. Heinrich, Challenges in tissue engineering – towards cell control inside artificial scaffolds, Soft Matter 12 (2016) 4287–4294.

[53] T. Volova, E. Kiselev, O. Vinogradova, E. Nikolaeva, A. Chistyakov, A. Sukovatiy, E. Shishatskaya, A glucose-utilizing strain, Cupriavidus euthrophus B-10646: growth kinetics, characterization and synthesis of multicomponent PHAs, PLoS One 9 (2014) e87551, , https://doi.org/10.1371/journal.pone.0087551.

[54] H.R. Recalde, A simple method of obtaining monocytes in suspension, J. Immunol. Methods 69 (1984) 71–77.

[55] R.B. Litman, R.J. Barrnett, The mechanism of the fixation of tissue components by osmium tetroxide via hydrogen bonding, J. Ultrastruct. Res. 38 (1972) 63–86.

[56] M.V. Berridge, A.S. Tan, Characterisation of the cellular reduction of 3-(4,5-dimethylthiazol-2yl)-2,5-diphenyltetrazolium bromide (MTT): subcellular localization, substrate dependence, and involvement of mitochondrial electron transport in MTT reduction, Arch. Biochem. Biophys 303 (1993) 474–482.

[57] M.V. Berridge, P.M. Herst, A.S. Tan, Tetrazolium dyes as tools in cell biology: new insights into their cellular reduction, Biotechnol. Annu. Rev. 11 (2005) 127–152.

[58] A.J. Freemerman, A.R. Johnson, G.N. Sacks, J.J. Milner, E.L. Kirk, M.A. Troester, A.N. Macintyre, P. Goraksha-Hicks, J.C. Rathmell, L. Makowski, Metabolic reprogramming of macrophages: glucose transporter 1 (GLUT1)-mediated glucose metabolism drives a proinflammatory phenotype, J. Biol. Chem. 289 (2014) 7884–7896.

[59] T.H. Tu, C.S. Kim, I.S. Nam-Goong, C.W. Nam, Y.I. Kim, T. Goto, T. Kawada, T. Park, J.H. Park, Z.Y. Ryoo, J.W. Park, H.S. Choi, R. Yu, 4-1BBL signaling promotes cell proliferation through reprogramming of glucose metabolism in monocytes/macrophages, FEBS J. 282 (2015) 1468–1480.

[60] J. Wang, Z. Duan, Z. Nugent, J.X. Zou, A.D. Borowsky, Y. Zhang, C.G. Tepper, J.J. Li, O. Fiehn, J. Xu, H.J. Kung, L.C. Murphy, H.W. Chen, Reprogramming metabolism by histone methyltransferase NSD2 drives endocrine resistance via coordinated activation of pentose phosphate pathway enzymes, Cancer Lett. 378 (2016) 69–79.

[61] F.Y. McWhorter, T. Wang, P. Nguyen, T. Chung, W.F. Liu, Modulation of macrophage phenotype by cell shape, Proc. Natl. Acad. Sci. U. S. A. 110 (2013) 17253–172538.

[62] T.U. Luu, S.C. Gott, B.W. Woo, M.P. Rao, W.F. Liu, Micro- and nanopatterned topographical cues for regulating macrophage cell shape and phenotype, ACS Appl. Mater. Interfaces 7 (2015) 28665–28672.

[63] L. Ziegler-Heitbrock, P. Ancuta, S. Crowe, M. Dalod, V. Grau, D.N. Hart, P.J. Leenen, Y.J. Liu, G. MacPherson, G.J. Randolph, J. Scherberich, J. Schmitz, K. Shortman, S. Sozzani, H. Strobl, M. Zembala, J.M. Austyn, M.B. Lutz, Nomenclature of monocytes and dendritic cells in blood, Blood 116 (2010) 74–80.

[64] S. Maharaj, K. Lu, S. Radom-Aizik, F. Zaldivar, F. Haddad, H.W. Shin, S.Y. Leu, E. Nussbaum, I. Randhawa, D.M. Cooper, Inter- and intra-subject variability of nitric oxide levels in leukocyte subpopulations, Nitric Oxide 72 (2018) 41–45.

[65] Z. Guła, M. Stec, M. Rutkowska-Zapała, M. Lenart, M. Korkosz, J. Gasowski, J. Baran, M. Baj-Krzyworzeka, R. Szatanek, J. Czyz, M. Siedlar, Number of circulating non-classical (CD14 + CD16 + +) monocytes negatively correlates with DAS28 and swollen joints count in peripheral spondyloarthritis patients, Pol. Arch. Intern. Med. 127 (2017) 846–853.

[66] K. Urbanski, D. Ludew, G. Filip, A. Sagan, P. Szczepaniak, G. Grudzien, J. Sadowski, B. Jasiewicz-Honkisz, T. Sliwa, B. Kapelak, E. McGinnigle, Y. Mikolajczyk, T.J. Guzik, CD14+CD16 + + "nonclassical" monocytes are associated with endothelial dysfunction in patients with coronary artery disease, Thromb. Haemost. 117 (2017) 971–980.

[67] D.R. Engel, J. Maurer, A. Tittel, C. Weisheit, T. Cavlar, B. Schumak, A. Limmer, A.N. van Rooijen, C. Trautwein, F. Tacke, C. Kurts, CCR2 mediates homeostatic and inflammatory release of Gr1 high monocytes from the bone marrow, but is dispensable for bladder infiltration in bacterial urinary tract infection, J. Immunol. 181 (2008) 5579–5586.

[68] C. Ulrich, B. Trojanowicz, R. Fiedler, F. Kohler, A.F. Wolf, E. Seibert, M. Girndt, Differential expression of lipoprotein-associated phospholipase A2 in monocyte subsets: impact of uremia and atherosclerosis, Nephron 135 (2017) 231–241.

[69] H.M. Makinde, C.M. Cuda, T.B. Just, H.R. Perlman, S.J. Schwulst, Nonclassical monocytes mediate secondary injury, neurocognitive outcome, and neutrophil infiltration after traumatic brain injury, J. Immunol. 199 (2017) 3583–3591.

[70] G. Thomas, R. Tacke, C.C. Hedrick, R.N. Hanna, Nonclassical patrolling monocyte function in the vasculature, Arterioscler. Thromb. Vasc. Biol. 35 (2015) 1306–1316.

[71] L. Garcia-Bonilla, G. Faraco, J. Moore, M. Murphy, G. Racchumi, J. Srinivasan, D. Brea, C. Iadecola, J. Anrather, Spatio-temporal profile, phenotypic diversity, and fate of recruited monocytes into the post-ischemic brain, J. Neuroinflamm. 13 (2016) 285.

[72] C.N. França, M.C. Izar, M.N. Hortêncio, J.B. Amaral, C.E.S. Ferreira, I.D. Tuleta, F.A.N. Fonseca, Monocyte subtypes and the CCR2 chemokine receptor in cardiovascular disease, Clin. Sci. 131 (2017) 1215–1224.

[73] A. Quintar, Mc.S. Ardle, D. Wolf, A. Marki, E. Ehinger, M. Vassallo, J. Miller, Z. Mikulski, K. Ley, K. Buscher, Endothelial protective monocyte patrolling in large arteries intensified by western diet and atherosclerosis, Circ. Res. 120 (2017) 1789–1799.

[74] U. Trahtemberg, A. Grau, A. Tabib, M. Atallah, A. Krispin, D. Mevorach, Identification and characterization of two human monocyte-derived dendritic cell subpopulations with different functions in dying cell clearance and different patterns of cell death, PLoS One 11 (2016) e0162984, , https://doi.org/10.1371/journal.pone.0162984.

[75] M. Wildgruber, T. Aschenbrenner, H. Wendorff, M. Czubba, A. Glinzer, B. Haller, M. Schiemann, A. Zimmermann, H. Berger, H.H. Eckstein, R. Meier, W.A. Wohlgemuth, P. Libby, A. Zernecke, The "intermediate" CD14+ + CD16+ monocyte subset increases in severe peripheral artery disease in humans, Sci. Rep. 6 (2016) 39483, https://doi.org/10.1038/srep39483.

[76] J. Yang, L. Zhang, C. Yu, X.F. Yang, H. Wang, Monocyte and macrophage differentiation: circulation inflammatory monocyte as biomarker for inflammatory diseases, Biomark. Res. 2 (2014) 1, https://doi.org/10.1186/2050-7771-2-1.

[77] A.A. Eekhoff, N. Bonakdar, J.L. Alonso, B. Hoffmann, W.H. Goldmann, Glomerular podocytes: a study of mechanical properties and mechano-chemical signaling, Biochem. Biophys. Res. Commun. 406 (2011) 229–233.

[78] D.E. Minner, P. Rauch, J. Käs, C.A. Naumann, Polymer-tethered lipid multi-bilayers: a biomembrane-mimicking subcell substrate to probe cellular mechano-sensing, Soft Matter 10 (2014) 1189–1198.

[79] J. Hong, S. Murugesan, E. Betzig, J.A. Hammer, Contractile actomyosin arcs promote the activation of primary mouse T cells in a ligand-dependent manner, PLoS One 12 (2017) e0183174, , https://doi.org/10.1371/journal.pone.0183174.

[80] F. Rey-Giraud, M. Hafner, C.H. Ries, In vitro generation of monocyte-derived macrophages under serum-free conditions improves their tumor promoting functions,

PLoS One 7 (2012) e42656, , https://doi.org/10.1371/journal.pone.0042656.

[81] F. Heinrich, A. Lehmbecker, B.B. Raddatz, K. Kegler, A. Tipold, V.M. Stein, A. Kalkuhl, U. Deschl, W. Baumgärtner, R. Ulrich, I. Spitzbarth, Morphologic, phenotypic, and transcriptomic characterization of classically and alternatively activated canine blood-derived macrophages in vitro, PLoS One 12 (2017) e0183572, , https://doi.org/10.1371/journal.pone.0183572.

[82] S. Fais, V.L. Burgio, M. Silvestri, M.R. Capobianchi, A. Pacchiarotti, F. Pallone, Multinucleated giant cells generation induced by interferon-gamma. Changes in the expression and distribution of the intercellular adhesion molecule-1 during macrophages fusion and multinucleated giant cell formation, Lab. Invest. 71 (1994) 737–744.

[83] L. Helming, J. Winter, S. Gordon, The scavenger receptor CD36 plays a role in cytokine-induced macrophage fusion, J. Cell. Sci. 122 (2009) 453–459.

[84] R.J. Miron, D.D. Bosshardt, Multinucleated giant cells: good guys or bad guys, Tissue Eng. Part B Rev. 24 (2017) 53–65.

[85] H. Moon, C.V. Cremmel, A. Kulpa, N.A. Jaeger, R. Kappelhoff, C.M. Overall, J.D. Waterfield, D.M. Brunette, Novel grooved substrata stimulate macrophage fusion, CCL2 and MMP-9 secretion, J. Biomed. Mater. Res. A. 104 (2016) 2243–2254.

[86] J.L. Collison, L.M. Carlin, M. Eichmann, F. Geissmann, M. Peakman, Heterogeneity in the locomotory behavior of human monocyte subsets over human vascular endothelium in vitro, J. Immunol. 195 (2015) 1162–1170.

[87] A. Haschemi, P. Kosma, L. Gille, C.R. Evans, C.F. Burant, P. Starkl, B. Knapp, R. Haas, J.A. Schmid, C. Jandl, S. Amir, G. Lubec, J. Park, H. Esterbauer, M. Bilban, L. Brizuela, J.A. Pospisilik, L.E. Otterbein, O. Wagner, The sedoheptulose kinase carkl directs macrophage polarization through control of glucose metabolism, Cell Metab. 15 (2012) 813–826.

[88] K. Bedard, K.H. Krause, The NOX family of ROS-generating NADPH oxidases: physiology and pathophysiology, Physiol. Rev. 87 (2007) 245–313.